Chemical Geology 469 (2017) 47–59

Contents lists available at ScienceDirect

Chemical Geology

journal homepage: www.elsevier.com/locate/chemgeo

The origin of the Zhubu mafic-ultramafic intrusion of the Emeishan large igneous province, SW China: Insights from volatile compositions and C-Hf-Sr-Nd isotopes

Qingyan Tang [a,*], Mingjie Zhang [a,*], Yuekun Wang [a], Yunsheng Yao [a], Li Du [b], Liemeng Chen [c], Zhongping Li [a,b]

[a] Key Lab of Mineral Resources in Western China (Gansu), School of Earth Sciences, Lanzhou University, Lanzhou 730000, China
[b] Key Lab of Petroleum Resource, Gansu Province/Key Lab of Petroleum Resources Research, CAS, Lanzhou 730000, China
[c] State Key Lab of Ore Deposit Geochemistry, Institute of Geochemistry, CAS, Guiyang 550002, China

ARTICLE INFO

Article history:
Received 28 July 2016
Received in revised form 4 February 2017
Accepted 6 February 2017
Available online 8 February 2017

Keywords:
Origins
C-Hf-Sr-Nd isotopes
Volatile compositions
Mafic-ultramafic rocks
Sulfide deposit
Emeishan LIP
SW China

ABSTRACT

The Zhubu mafic-ultramafic intrusion of the Permian Emeishan large igneous province (LIP), SW China hosts a magmatic Ni, Cu and platinum-group element (PGE) deposit. It consists of a layered sequence with sub-horizontal modal layering wrapped by a sub-vertical marginal zone. Our new zircon U-Pb isotopic dating gives a mean age of 263.2 ± 5.6 Ma for the layered sequence. The volatiles extracted from the mineral separates of the Zhubu intrusion are composed of predominant H_2O (11,769.84 $mm^3 \cdot STP/g$, STP-standard temperature and pressure) and minor H_2 and CO_2. The layered sequence has lower H_2O but higher H_2, CO_2, H_2S and SO_2 contents than the marginal zone. The CO_2 and CH_4 extracted at 400–900 °C and 900–1200 °C have light $\delta^{13}C_{CO2}$ varying from −17.45‰ to −7.10‰ and $\delta^{13}C_{CH4}$ varying from −41.35‰ to −22.88‰. The pyroxene separates have significantly lower $(^{87}Sr/^{86}Sr)_i$ values (0.705882 to 0.708912) and slightly higher ε_{Nd} (t = 263 Ma) values (−2.8 to 0.7) than the whole rocks. The ε_{Hf} (t = 263 Ma) values of zircon crystals vary from −3.05 to +1.90. The chemical compositions of volatiles from the Zhubu intrusion indicate a slightly reduced condition and a H_2O-rich parental magma. The C-Hf-Sr-Nd isotopes for the Zhubu intrusion are consistent with ~15 wt% assimilation of the upper crust by a mantle-derived magma. The carbon isotopes indicate that a thermogenic component from sedimentary organic materials was present in the contaminated magma. A weak positive correlation between volatile and PGE contents, together with the C-Hf-Sr-Nd isotopes, indicates that sulfide saturation in the Zhubu magma was triggered by crustal contamination including the addition of volatiles.

1. Introduction

Permian mantle plume activity produced the world-class magmatic Fe-Ti-V oxide deposits in the Emeishan LIP, SW China, and the Ni-Cu-PGE sulfide deposits in the Siberian LIP in Russia. These two types of magmatic deposits in the different LIPs formed in distinct redox conditions, i.e., different volatile compositions (Li et al., 2003, 2009, 2012, 2016; Wang et al., 2006, 2007; Zhang et al., 2006, 2008, 2013a; Hou et al., 2011, 2012; Xing et al., 2012; Tang et al., 2013a). Generally, magmatic oxide deposits are formed under high oxygen fugacity environment (Hou et al., 2012; Xing et al., 2012), whereas sulfide deposits are formed in reduced condition (Jugo et al., 2005; Li et al., 2009; Fu et al., 2012; Tang et al., 2013b). Meanwhile, sulfur saturation in mafic magma is required for the formation of Ni-Cu-PGE sulfide deposits (e.g., Keays and Lightfoot, 2010). The most common cause of this process is crustal contamination including the addition of external sulfur (Ripley and Li, 2013). The actual mechanisms involved include volatile and sulfur transfer (Robertson et al., 2015). The Emeishan LIP formed Ni-Cu-PGE sulfide deposits and world-class magmatic Fe-Ti-V oxide deposits, and provides an insight into the volatile condition and sulfur saturation.

Important magmatic Ni-Cu-PGE sulfide deposits commonly form in conduit and in situ crystallization magmatic systems (Li et al., 2009). The Zhubu mafic-ultramafic intrusion is composed of a layered sequence and a marginal zone, that were formed in an early conduit stage and a late *in situ* differentiation stage, respectively in the Emeishan LIP (Tang et al., 2013b). The Zhubu intrusion contains important sulfide deposits in the marginal zone and small sulfide lenses in the layered sequence. Therefore, it is an ideal intrusion for sulfide mineralization in conduit and *in situ* crystallization systems in the Emeishan LIP. Previous studies concluded that sulfide saturation in the Zhubu magmatic system was triggered by crustal contamination (e.g., Tang et al., 2013b). However, the actual mechanism and the possibility of sulfur transfer by volatiles are still unclear.

Constraints on the sources of volatiles are critical for determining the overall volatile budget, the role of crustal assimilation and the evolution

* Corresponding authors.
E-mail addresses: tangqy@lzu.edu.cn (Q. Tang), mjzhang@lzu.edu.cn (M. Zhang).

http://dx.doi.org/10.1016/j.chemgeo.2017.02.009
0009-2541/

of sulfide-mineralized mafic magma. The chemical compositions and carbon isotopic compositions of volatiles from minerals have been used to study the sources of volatiles in magmatic deposits (Fu et al., 2012; Xing et al., 2012; Zhang et al., 2013a). Sr-Nd isotopes of pyroxene or whole rocks and Hf isotopes of zircons provide critical constrains on siliceous crustal contamination. In this paper, the chemical and C isotopic compositions of volatiles, the U-Pb and Hf isotopes of zircon and the Sr-Nd isotopes of pyroxene separates from the Zhubu mafic-ultramafic intrusion are reported to better understand the composition and origin of the volatiles in the Zhubu intrusion, Emeishan LIP, compared with the Fe-Ti-V oxide deposits (Xing et al., 2012).

2. Geological background

2.1. Regional geology

The Emeishan LIP covers an area of ~2.5×10^5 km^2 from the western part of the Yangtze Block in SW China and to northern Vietnam. It is composed predominantly of Permian flood basalts with temporally and spatially associated intrusions with compositions varying from mafic-ultramafic rocks to syenites and granites. The mafic-ultramafic intrusions such as the Panzhihua, Taihe, Hongge and Baima intrusions host giant Fe-Ti-V oxide deposits whereas the Zhubu, Limahe and Baimazhai intrusions host Ni-Cu-PGE sulfide deposits (Fig. 1a). Country rocks to these intrusions are Ordovician–Devonian sandstones or limestones (Zhou et al., 2005, 2008). The zircon U-Pb ages of these intrusions and the associated basalts vary from ~259 Ma to ~263 Ma (Fan et al., 2008; Zhou et al., 2008; Zhong et al., 2011, 2014; Tang et al., 2015). These intrusions and basalts are believed to have been formed by a Permian Emeishan mantle plume (Xu et al., 2004, 2007).

2.2. Geology of the Zhubu intrusion

The Zhubu mafic-ultramafic intrusion is located in the central part of the Emeishan LIP and hosts a magmatic Cu–Ni–PGE sulfide deposit (Zhou et al., 2008; Tang et al., 2013b) (Fig. 1a, b). It is ~750 m long and ~400 m wide with downward extension >580 m (Fig. 1c). The Zhubu intrusion intruded the Precambrian meta-sedimentary rocks. It is composed of a central layered sequence wrapped by a marginal zone. The marginal zone is discordant with the layered sequence (Fig. 1c), and no chilled rocks are present between the marginal zone and the layered sequence. A hornfels zone of 0.5–1 m in thickness is present between the marginal zone and the country rocks.

The layered sequence constitutes >90% of the total volume of the intrusion and is characterized by sub-horizontal modal layering. Lherzolite and olivine websterite occur at the bottom, and gabbro and gabbro-diorite occur at the top (Fig. 1c). The different rock units in the entire layered sequence have gradational contacts. The marginal zone is ~10 to 40 m across. It is composed of lherzolite, olivine websterite, websterite and contaminated gabbroic rocks. Small country rock xenoliths (<10 cm in diameter) are present in places in the gabbroic rocks. The SHRIMP zircon U-Pb dating yielded 261 ± 2 Ma for diorite from the marginal zone of the Zhubu intrusion (Zhou et al., 2008).

The most important sulfide mineralization in the Zhubu intrusion occurs mainly as disseminated sulfides (pyrrhotite, pentlandite and chalcopyrite) within the marginal zone. Small lenses of disseminated sulfides are also present within the layered sequence, but they are

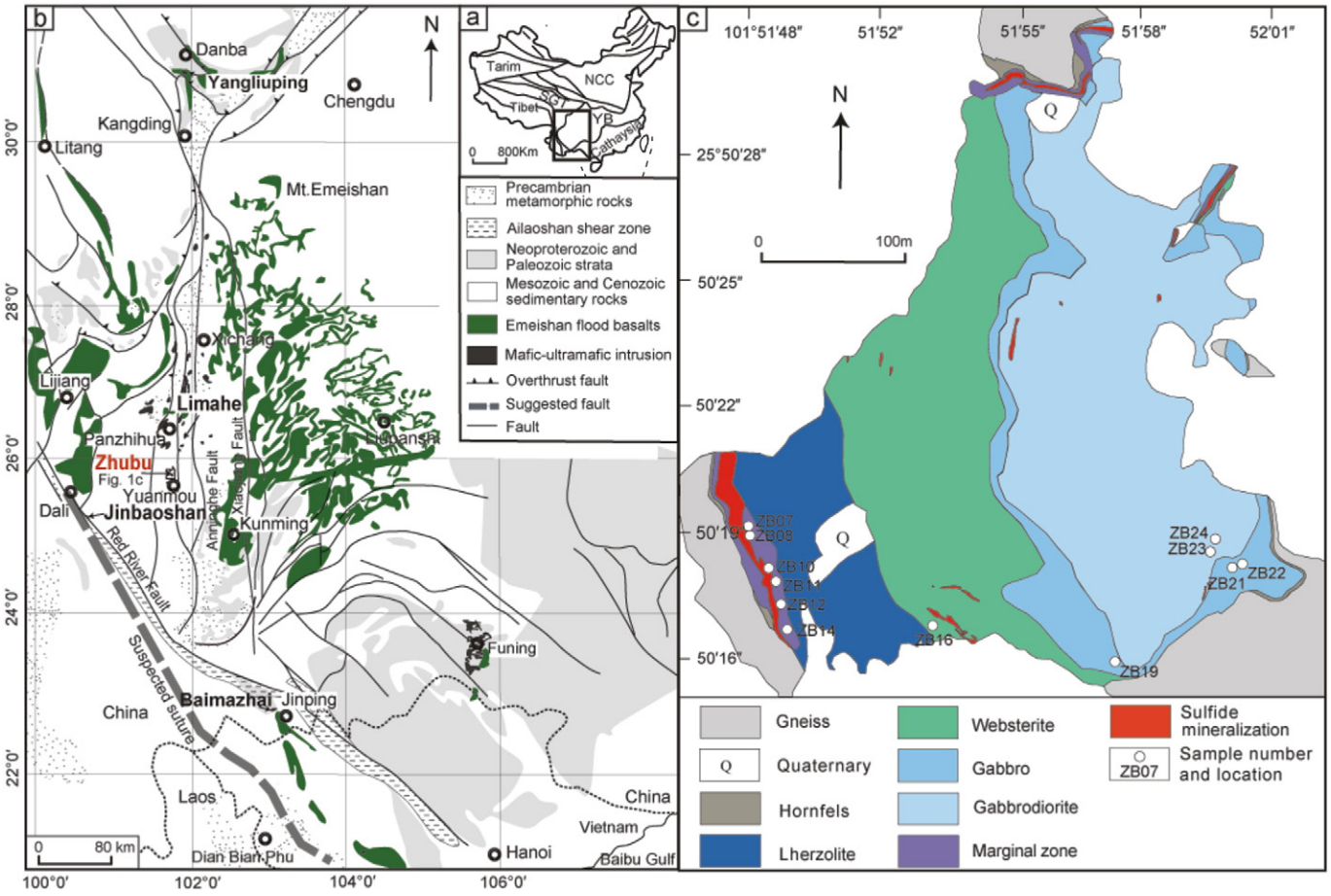

Fig. 1. The distribution of Emeishan flood basalts and associated mafic-ultramafic intrusions (a, b) and simplified geologic map (c) of the Zhubu mafic-ultramafic intrusion, China (modified from Chung and Jahn, 1995; Song et al., 2001; Tang et al., 2013a, b). NCC = north China craton, SGT = Songpan-Ganzi terrane, YB = Yangtze block.

volumetrically insignificant. The Ni and Cu grades are as high as 0.8 wt%, and the Pt and Pd grades reach 3 ppm (Tang et al., 2013b).

3. Samples and analytical methods

3.1. Samples and sample pretreatment

The samples used in this study were collected from an open pit and the outcrops of the Zhubu intrusion. Six lherzolite (Lht) and olivine websterite (OlWs) samples were collected from the marginal zone in the western part of the intrusion, and five olivine gabbro (OlGb), gabbro (Gbr) and gabbro-diorite (Gbdt) samples were collected from the outcrops of layered sequence of the intrusion. Sample locations are shown in Fig. 1c. The whole-rock geochemical and Sr-Nd isotopic data were reported in Tang et al. (2013b).

Lherzolite contains 40–60% (modal) olivine and 30–40% pyroxenes, plus minor hornblende and phlogopite. Small chromite crystals and sulfide inclusions are present in some olivine crystals. Olivine is a cumulus phase, and pyroxenes, hornblende and phlogopite occur in the interstitial spaces. Olivine websterite contains 20–30% olivine, 50–60% pyroxenes, and minor amounts of plagioclase, hornblende and phlogopite. Olivine crystals are commonly enclosed in large orthopyroxene crystals in olivine websterite. Gabbro contains <5% olivine, 40–45% pyroxenes, 40–50% plagioclase, and minor hornblende and phlogopite. Gabbrodiorite contains 30–40% plagioclase, 15–25% clinopyroxene, 20–30% hornblende, 5–10% biotite and 10–15% Fe-Ti oxides. Partial alterations of olivine by serpentine + magnetite; orthopyroxene by talc; clinopyroxene by actinolite, tremolite or chlorite; and plagioclase by sericite + epidote + albite are present in the samples. Disseminated sulfides are partially replaced by secondary magnetite in some samples.

Zircon grains from a gabbro in the layered sequence of the Zhubu intrusion were separated using conventional methods including elutriation, heavy liquids and magnetic separation. They were carefully hand-picked under a binocular microscope and then mounted in epoxy and polished down to their cores for U-Pb dating and Hf isotopic analysis (Zhang et al., 2010; Tang et al., 2015). Cathodoluminescence images were used for textural observation and target selection for U-Pb and Hf isotopic analysis.

Pyroxene crystals provide more-robust Nd and Sr isotopic constraints on the parent magmas and their magma sources (Revillon et al., 2002). Although they have lower concentrations of Rb, Sr, Sm and Nd than whole rocks, Rb and Sr in pyroxenes are commonly less affected by post-magmatic hydrothermal alteration than in whole rocks. One olivine and ten pyroxene mineral separates were hand-picked from the selected samples under a binocular microscope. The selected samples are the least altered among the samples we collected from the Zhubu intrusion. The mineral separates were immersed in 0.3 mol/L HCl for 24 h to remove possible carbonates and soluble alteration parts that may occur in micro-fractures and cleavages. They were then washed using distilled water until the pH value of the rinsing water reached ~7. Finally they were cleaned ultrasonically with CH_2Cl_2 to remove possible surface organic contaminants. The cleaned samples were baked at 110 °C prior to analysis (Zhang et al., 2007, 2013a). A total of 10 mineral separates from the Zhubu intrusion were used for volatile and C-Sr-Nd isotopic analysis.

3.2. Analytical methods

The chemical compositions of the volatiles in the olivine and pyroxene separates from the Zhubu intrusion were determined using a MAT-271 mass spectrometer connected to a vacuum stepwise heating system at the Key Laboratory of Gas Geochemistry, Chinese Academy of Sciences, Lanzhou, China. The volatile extraction procedures and chemical analysis are described in detail by Zhang et al. (2007) and Tang et al. (2013a). The sample was heated from 200 °C to 1200 °C in 100 °C increments and 1 h duration at each step to extract volatiles from the sample for chemical composition analysis. The analytical errors were <1 vol% relative for CO_2, CO and H_2; <5 vol% for H_2O and <10 vol% for other minor volatiles (Zhang et al., 2007, 2009).

Carbon isotopes of CO_2 and CH_4, which can be expressed as $\delta^{13}C$ (‰) = $([^{13}C/^{12}C]_{sample} / [^{13}C/^{12}C]_{PDB} - 1) \times 10^3$ (where PDB, Pee Dee Belemnite, is the reference standard), were analyzed by a Gas chromatography-Combustion-Mass spectrometer system using a stepwise-heating extraction procedure at the Key Laboratory of Gas Geochemistry, CAS, Lanzhou, China. CO_2 and CH_4 extracted at 200–400 °C, 400–900 °C and 900–1200 °C intervals, respectively were analyzed for the analysis of carbon isotopic compositions based on the releasing patterns of the volatiles (see result for details). The CO_2 and CH_4 were separated by an Agilent 6890N gas chromatographic analyzer, oxidized into CO_2, then sent into a Delta plus XP mass spectrometer for carbon isotopic analysis. The reported $\delta^{13}C$ values (relative to PDB) have a relative error <1.6‰. The details of CO_2 and CH_4 extractions and measurements are given in Zhang et al. (2007).

Zircon U–Pb and Lu-Hf isotope measurements were performed using a Neptune multi-collector ICP-MS equipped with a New Wave UP 213 laser-ablation sampling system at the MRL Key Laboratory of Metallogeny and Mineral Assessment, Institute of Mineral Resources, Chinese Academy of Geological Sciences, Beijing, China. The analytical procedures and operation conditions are given in Hou et al. (2009), Wu et al. (2006) and Tang et al. (2014). The laser beam size was approximately 40–50 μm in diameter. The GJ1 zircon standard was used as a reference. The plotting and age calculations are from Isoplot/Ex 3.00 (Ludwig, 2003).

Rb–Sr and Sm–Nd isotopes of the pyroxene separates were determined using a Triton thermal ionization magnetic sector mass spectrometer at the Institute of Geology and Mineral Resources in Tianjin, CGS, China. The powders were treated with 0.3 N HCl for 1 h at ~100 °C and were then dried after rinsing with purified water. The samples were weighed and spiked with mixed isotope tracers and dissolved in Teflon capsules with HF + HNO_3 at 120 °C for 7 days. The procedural blanks were <100 pg for Sm and Nd, and <500 pg for Rb and Sr. The mass fractionation corrections for the Sr and Nd isotopic ratios were based on the following values: $^{86}Sr/^{88}Sr = 0.1194$ and $^{146}Nd/^{144}Nd = 0.7219$. The typical within-run precision (2σ) for Sr and Nd isotopic ratios is less than ±0.5% relative. The measured values for the LRIG Nd standard and the NBS987 Sr standard were $^{143}Nd/^{144}Nd = 0.512202 \pm 25$ and $^{87}Sr/^{86}Sr = 0.710245 \pm 35$ during the period of data acquisition. The analytical procedures and operation conditions are given in Zhang et al. (2011).

4. Results

4.1. Zircon U-Pb age

The U–Pb data of zircon grains from the Zhubu gabbro are listed in Table 1. The Th/U ratios of the zircon crystals are between 2.39 and 4.62 (Table 1), which are within the range of typical igneous zircons (Hoskin and Schaltegger, 2003). The concordia plot for the analyzed zircons is illustrated in Fig. 2. The zircon grains from the Zhubu gabbro have $^{206}Pb/^{238}U$ ages varying from 255 Ma to 291 Ma (Table 1). The eight youngest zircon crystals yield a weighted mean $^{206}Pb/^{238}U$ age of 263.2 ± 5.6 Ma for the gabbro of the layered sequence, which is identical (i.e., within the analytical errors) to the SHRIMP zircon U-Pb age of 261 ± 2 Ma for the diorite from the marginal zone of the Zhubu intrusion (Zhou et al., 2008).

4.2. Chemical and carbon isotopic compositions of volatiles

The volatiles of silicate minerals from the Zhubu intrusion were released with elevated temperature at three temperature intervals: 200–400 °C, 400–900 °C and 900–1200 °C (Fig. 3a). Summations of the volatile contents at the three temperature intervals are listed in Table 2. The original data are given as supplementary materials in Table S1.

Table 1
The LA-MC-ICP-MS U-Pb data of zircon crystals from gabbro in the Zhubu intrusion.

Spot analysis	Pb (ppm)	Th (ppm)	U (ppm)	Th/U	$^{207}Pb/^{206}Pb$ Ratio	1σ	$^{207}Pb/^{235}U$ Ratio	1σ	$^{206}Pb/^{238}U$ Ratio	1σ	$^{207}Pb/^{206}Pb$ Age (Ma)	1σ	$^{207}Pb/^{235}U$ Age (Ma)	1σ	$^{206}Pb/^{238}U$ Age (Ma)	1σ	Conc. (%)
ZB11-19-01	598.69	565.59	204.52	2.77	0.052975	0.000992	0.301292	0.009334	0.041218	0.000985	327.8	42.6	267.4	7.3	260.4	6.1	97
ZB11-19-02	444.56	421.51	155.63	2.71	0.053653	0.000847	0.298287	0.005639	0.040335	0.000474	366.7	35.2	265.1	4.4	254.9	2.9	96
ZB11-19-03	863.87	780.70	242.47	3.22	0.052025	0.000637	0.307676	0.007382	0.042853	0.000785	287.1	32.4	272.4	5.7	270.5	4.9	99
ZB11-19-04	544.37	565.92	184.02	3.08	0.053089	0.000705	0.300452	0.005433	0.041087	0.000655	331.5	29.6	266.8	4.2	259.6	4.1	97
ZB11-19-05	1555.92	1567.83	342.02	4.58	0.052243	0.000624	0.306140	0.007579	0.042471	0.000871	294.5	-4.6	271.2	5.9	268.1	5.4	98
ZB11-19-06	1316.56	1462.17	316.79	4.62	0.052370	0.000694	0.308067	0.007950	0.042740	0.001113	301.9	-0.9	272.7	6.2	269.8	6.9	98
ZB11-19-07	460.85	603.41	167.89	3.59	0.050144	0.000778	0.303362	0.007722	0.043938	0.001009	211.2	37.0	269.0	6.0	277.2	6.2	97
ZB11-19-08	651.08	812.22	217.81	3.73	0.052501	0.000822	0.308057	0.009412	0.042479	0.000972	305.6	35.2	272.7	7.3	268.2	6.0	98
ZB11-19-10	406.31	542.37	156.39	3.47	0.051731	0.000873	0.312898	0.006779	0.043849	0.000444	272.3	43.5	276.4	5.2	276.6	2.7	99
ZB11-19-11	321.85	421.52	125.67	3.35	0.051898	0.001035	0.323066	0.007411	0.045212	0.000629	279.7	44.4	284.3	5.7	285.1	3.9	99
ZB11-19-12	382.90	553.44	152.67	3.63	0.051507	0.000815	0.327341	0.006165	0.046122	0.000441	264.9	32.4	287.5	4.7	290.7	2.7	98
ZB11-19-13	378.03	567.78	157.82	3.60	0.054113	0.000881	0.336714	0.006085	0.045181	0.000418	376.0	37.0	294.7	4.6	284.9	2.6	96
ZB11-19-14	260.04	415.49	143.14	2.90	0.050674	0.000961	0.309839	0.007215	0.044351	0.000451	233.4	72.2	274.1	5.6	279.7	2.8	97
ZB11-19-15	301.36	501.58	148.23	3.38	0.051677	0.001032	0.327220	0.007225	0.045987	0.000463	333.4	41.7	287.4	5.5	289.8	2.9	99
ZB11-19-16	436.57	596.41	141.49	4.22	0.052966	0.001051	0.332533	0.008373	0.045567	0.000644	327.8	44.4	291.5	6.4	287.2	4.0	98
ZB11-19-17	406.36	517.21	149.42	3.46	0.050618	0.001029	0.315192	0.007256	0.045195	0.000445	233.4	78.7	278.2	5.6	285.0	2.7	97
ZB11-19-18	302.98	345.24	106.46	3.24	0.051379	0.001123	0.314360	0.007968	0.044418	0.000587	257.5	50.0	277.6	6.2	280.2	3.6	99
ZB11-19-19	1330.79	1426.11	335.17	4.25	0.050824	0.000648	0.314981	0.005959	0.044948	0.000486	231.6	25.0	278.0	4.6	283.4	3.0	98
ZB11-19-20	676.75	662.38	193.24	3.43	0.057382	0.005443	0.347739	0.034608	0.043835	0.000364	505.6	209.2	303.0	26.1	276.6	2.2	90
ZB11-19-21	875.50	819.97	244.32	3.36	0.051611	0.000687	0.316600	0.005239	0.044510	0.000388	333.4	29.6	279.3	4.0	280.7	2.4	99
ZB11-19-22	225.93	163.43	68.33	2.39	0.051827	0.001371	0.303482	0.008622	0.042536	0.000537	276.0	63.9	269.1	6.7	268.5	3.3	99
ZB11-19-23	779.71	658.04	185.39	3.55	0.052146	0.000675	0.317787	0.005262	0.044224	0.000457	300.1	29.6	280.2	4.1	279.0	2.8	99
ZB11-19-24	648.80	506.01	167.40	3.02	0.050873	0.000900	0.306267	0.006171	0.043692	0.000446	235.3	40.7	271.3	4.8	275.7	2.8	98
ZB11-19-25	1168.17	874.87	237.80	3.68	0.051827	0.000879	0.314690	0.005904	0.044082	0.000462	276.0	38.9	277.8	4.6	278.1	2.9	99

The volatiles in the Zhubu mineral separates were released predominantly at the 400–900 °C and 900–1200 °C intervals, and mildly at the 200–400 °C interval. The average contents of the total volatiles are av. 10,142.7, 2,500.2 and 566.61 $mm^3 \cdot STP/g$ (STP = standard temperature and pressure, the same hereinafter) for above three temperature intervals, respectively. The average contents of the total volatiles in the Zhubu minerals are av. 13,209.47 $mm^3 \cdot STP/g$, which are much higher than those in the minerals from the gabbro of the Siberian LIP (av. 5233.9 $mm^3 \cdot STP/g$) (Tang et al., 2013a). The conspicuous characteristics of the volatiles in the Zhubu samples are that H_2O is a dominant component (av. 11,769.84 $mm^3 \cdot STP/g$) in total volatiles. H_2O was released mainly at the 500–800 °C and 900–1100 °C intervals (Fig. 3b). The H_2O content in total volatiles from the minerals are av. 17,229.3 and 5867.4 $mm^3 \cdot STP/g$ for the lherzolite and olivine websterite of the marginal zone, respectively, and av. 4723.9, 15712.0 and 5600.7 $mm^3 \cdot STP/g$ for the olivine gabbro, gabbro and gabbrodiorite of the layered sequence, respectively.

The minor volatiles released from the Zhubu samples are composed of H_2 and CO_2 (av. 418.3 and 227.5 $mm^3 \cdot STP/g$, respectively). The CO_2 contents of the Zhubu intrusion are within the range for coeval mafic intrusions that host magmatic Fe-Ti-V oxide deposits in the Emeishan LIP (Xing et al., 2012). The total amounts of SO_2 and H_2S in the volatiles extracted from the Zhubu mineral separates increase from lherzolite, to olivine websterite, to olivine gabbro and to gabbro in accordance with the magmatic crystallizing sequence.

The volatiles extracted from the mineral separates from the Zhubu intrusion at different temperature intervals have different chemical compositions. The volatiles at the 200–400 °C interval are composed predominantly of H_2O (av. 507.57 $m^3 \cdot STP/g$), with minor amounts of CO_2 (av. 16.82), C_2H_6 (16.34) and N_2 (16.03). The volatiles at the 400–900 °C interval are dominated by H_2O (av. 9393.78 $mm^3 \cdot STP/g$), with minor amounts of H_2 (av. 400.50) and CO_2 (av. 186.28). The volatiles at the 900–1200 °C interval are also dominated by H_2O (av. 2376.07 $mm^3 \cdot STP/g$), with minor amounts of CO_2 (av. 35.99), SO_2 (26.28), O_2 (25.53) and H_2S (12.57).

The carbon isotopic compositions of CO_2 and CH_4 released from pyroxene separates in the Zhubu intrusion are listed in Table 3. The CO_2 released at the 900–1200 °C interval has $\delta^{13}C_{CO2}$ values ranging from −13.2‰ to −7.1‰ (av. −11.1‰). The volatiles released at the 400–900 °C interval have $\delta^{13}C_{CO2}$ varying from −17.5‰ to −7.3‰ (av. −10.5‰) and $\delta^{13}C_{CH4}$ varying from −41.3‰ to −22.9‰ (av. −31.8‰). In contrast, the volatiles at the 200–400 °C interval have significantly lower $\delta^{13}C_{CO2}$ (−24.5‰ to −13.0‰, av. −18.8‰) and $\delta^{13}C_{CH4}$ (−48.8‰ to −28.3‰, av. −40.5‰) values than those at 400–900 °C.

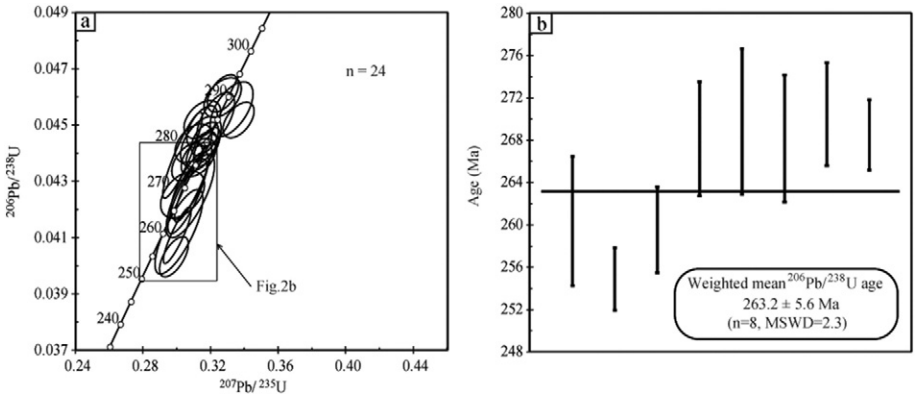

Fig. 2. U–Pb isotope concordia diagram (a) with a weighted mean $^{206}Pb/^{238}U$ age for the eight youngest comagmatic gabbro zircons (b) from the Zhubu intrusion, SW China.

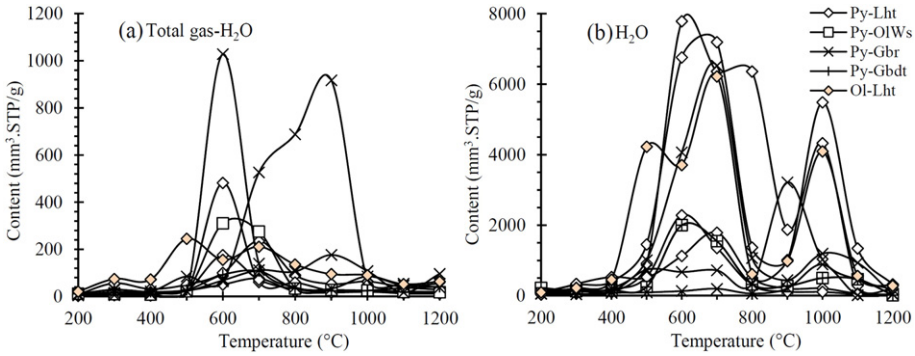

Fig. 3. The total contents of volatiles after deduction of water (a) and the H_2O contents (b) released from different temperatures in the olivine (Ol) and pyroxene (Py) separates from the Zhubu intrusion.

A weak positive correlation exists between $\delta^{13}C_{CO2}$ and the CO_2 content, but it does not correspond to the Rayleigh fractionation of carbon isotopes (Fig. 4a). The $\delta^{13}C$ values of CO_2 and CH_4 are between the mantle and crustal values (Fig. 4b, Ueno et al., 2006).

4.3. Sr, Nd and Hf isotopes

The Sr and Nd isotopes of pyroxene separates from the Zhubu intrusion are listed in Table 4. The concentrations of Rb, Sr, Sm and Nd in the pyroxene separates are lower than in whole rocks. The $(^{87}Sr/^{86}Sr)_i$ values vary from 0.705882 to 0.708912. The ε_{Nd} (t = 263 Ma) values (−2.8–0.7) are within the range of the Emeishan basalts and picrites (Chung and Jahn, 1995; Xu et al., 2001; Xiao et al., 2004; Zhang et al., 2006, 2008; Hou et al., 2012; Li et al., 2012). Fig. 5 shows a comparison of several coeval Ni-Cu sulfide-bearing mafic-ultramafic intrusions and Fe-Ti-V oxide ore-bearing mafic intrusions of the Emeishan LIP. The pyroxene separates in the Zhubu intrusion are characterized by significantly low $(^{87}Sr/^{86}Sr)_i$ and slightly high ε_{Nd} (t = 263 Ma) compared with their whole rock samples (Zhou et al., 2008; Tang et al., 2013b) (Fig. 5). The pyroxene separates from the Zhubu intrusion have $(^{87}Sr/^{86}Sr)_i$ and ε_{Nd} values similar to those for the whole-rock samples from other coeval Ni-Cu-PGE sulfide-bearing mafic-ultramafic intrusions, but they display slightly higher $(^{87}Sr/^{86}Sr)_i$ and lower ε_{Nd} than the coeval Fe-Ti-V oxide-bearing mafic intrusions in the Emeishan LIP.

The Lu-Hf isotopes of the eight youngest zircon crystals from the Zhubu gabbro are listed in Table 5. The calculated ε_{Hf} (t) values for the zircon grains from the Zhubu gabbro vary from −3.05 to +1.90. These values are slightly lower than those for the zircon crystals from the coeval Fe-Ti oxide-bearing mafic intrusions and basaltic andesite of the Emeishan LIP (Zhong et al., 2009, 2011; Shellnutt et al., 2015; Tang et al., 2015) (Fig. 6).

Table 2
Volatile chemical compositions ($mm^3 \cdot STP/g$) in the olivine and pyroxene separates in the Zhubu intrusion.

No.	Rock type	Mineral	Weight/g	T(°C)	H_2	CH_4	H_2O	CO	N_2	C_2H_6	O_2	H_2S	CO_2	SO_2
ZB11-07	Lherzolite	Ol	0.3	200–400	12.69	4.22	766.67	8.45	39.36	68.46	2.11	–	32.26	–
				400–900	273.99	35.67	15,747.37	99.90	59.03	36.23	41.80	30.75	262.09	–
				900–1200	51.82	–	4936.84	20.27	27.57	–	34.77	10.33	49.28	12.09
ZB11-07	Lherzolite	Py	0.48	200–400	3.83	–	800.44	0.65	44.88	27.67	2.35	–	17.66	–
				400–900	144.30	5.54	17,782.35	114.49	85.86	–	51.40	24.00	103.46	–
				900–1200	–	–	7144.74	8.04	18.19	–	33.62	5.05	45.62	21.06
ZB11-08	Lherzolite	Py	0.51	200–400	–	–	306.50	1.22	6.58	–	0.95	–	4.66	–
				400–900	537.89	0.24	23,291.54	8.93	8.43	0.00	21.62	24.07	43.94	–
				900–1200	–	–	4802.37	1.78	3.10		8.56	6.05	23.40	3.87
ZB11-10	Lherzolite	Py	0.47	200–400	2.99	0.18	893.06	1.95	7.70	12.59	0.94	–	16.20	–
				400–900	51.65	2.26	4142.22	7.15	5.25	0.50	11.92	12.15	99.76	–
				900–1200	–	–	301.23	1.29	4.89	0.92	13.59	8.54	32.00	3.98
ZB11-11	Lherzolite	Py	0.49	200–400	3.61	0.35	485.50	5.16	6.88	13.32	0.70	–	11.34	–
				400–900	231.64	1.02	4570.35	31.15	42.35	–	7.70	–	7.83	–
				900–1200	–	–	175.08	6.14	39.00	–	3.94	–	3.55	–
ZB11-14	Lherzolite	Py	0.5	200–400	41.88	4.68	538.42	–	75.60	13.18	0.22	–	3.39	–
				400–900	283.06	6.97	9927.37	61.26	141.50	–	37.73	–	–	–
				900–1200	–	–	520.00	27.62	46.24	–	29.82	–	–	–
ZB11-12	Olivine websterite	Py	0.51	200–400	9.23	0.26	744.58	0.35	23.10	–	3.11	1.42	14.13	–
				400–900	139.38	0.43	4142.93	22.88	31.08	–	19.76	19.93	413.89	–
				900–1200	–	–	979.88	–	10.15	0.00	17.25	9.34	14.17	11.29
ZB11–16	Olivine gabbro	Pyx	0.50	200–400	5.50	–	178.95	1.11	4.33	5.54	0.68	0.00	3.89	–
				400–900	327.61	0.24	685.79	17.93	8.71	–	35.97	47.44	44.99	–
				900–1200	2.21	–	947.37	9.41	6.01	0.71	56.56	47.60	34.40	62.63
ZB11–21	Olivine gabbro	Pyx	0.52	200–400	0.62	–	305.67	8.57	6.74	13.71	0.86	0.00	29.21	–
				400–900	1884.10	0.73	5676.11	88.97	8.86	0.26	61.07	77.77	156.98	0.16
				900–1200	0.75	–	1654.89	2.67	2.11	12.14	23.80	7.20	62.50	9.44
ZB11–22	Gabbro	Py	0.53	200–400	0.74	–	440.42	1.35	4.89	1.28	2.22	0.20	25.03	0.53
				400–900	321.25	4.20	13,106.26	22.63	12.44	0.00	122.90	152.45	604.35	14.29
				900–1200	–	–	2165.34	2.56	2.43	0.00	41.38	8.24	26.49	104.36
ZB11–23	Gabbrodiorite	Py	0.50	200–400	3.85	0.23	153.92	3.73	15.81	20.85	1.66	–	13.78	–
				400–900	93.23	3.07	4792.83	8.15	8.87	–	20.88	23.60	125.56	0.33
				900–1200	–	–	653.98	0.25	8.39	0.69	25.18	8.92	25.82	33.51

Note: Ol = olivine, Py = pyroxene, — = not determined.

Table 3
The carbon isotopic compositions (‰, v-PDB) of CO_2 and CH_4 released from pyroxene separates in the Zhubu intrusion.

		$\delta^{13}C_{CO2}$			$\delta^{13}C_{CH4}$	
Sample No.	Rock type	200–400 °C	400–900 °C	900–1200 °C	200–400 °C	400–900 °C
ZB11-07	Lherzolite	−21.55		−10.31	−44.39	−35.24
ZB11-08	Lherzolite	−22.83	−17.45	−10.42	−46.00	−27.84
ZB11-10	Lherzolite	−14.37	−10.30	−12.63	−28.28	−22.88
ZB11-11	Lherzolite	−14.84		−11.05	−33.66	−31.10
ZB11-14	Lherzolite	−20.68		−12.69	−43.11	−30.42
ZB11-12	Olivine websterite	−17.58	−7.26	−11.75	−47.58	−37.28
ZB11-16	Olivine gabbro	−20.94	−9.47	−9.52	−36.63	−30.22
ZB11-21	Olivine gabbro		−7.65	−7.10	−48.81	−41.35
ZB11-22	Gabbro	−14.99		−13.19	−29.80	−28.75
ZB11-23	Gabbro diorite	−21.36	−10.83	−12.75	−46.90	−32.65

5. Discussion

Mantle plume activity is important for the formation of magmatic Ni-Cu-PGE sulfide deposits, such as the world-class Ni-Cu-PGE sulfide deposits hosted in the mafic-ultramafic intrusions of the Siberian LIP in Russia. In the Emeishan LIP, only a few small magmatic sulfide deposits have been found to date, such as the Zhubu deposit (Tang et al., 2013b). Our new zircon U-Pb age for the layered sequence and the previously reported zircon age for the marginal zone confirm that the Zhubu mafic-ultramafic intrusion is one of many mafic-ultramafic intrusions of the Permian Emeishan LIP in SW China (Fan et al., 2008; Zhou et al., 2008; Zhong et al., 2011).

The pyroxene samples in the Zhubu intrusion are slightly scattered in $(^{87}Sr/^{86}Sr)_i$ values compared with the whole rock samples, implying that Sr isotope varied during pyroxene crystallization stage of different type of rocks, while the whole rock samples make Sr isotope homogenization. The pyroxene separates show significantly lower $(^{87}Sr/^{86}Sr)_i$ and slightly higher ε_{Nd} (t = 263 Ma) values compared with the whole rock samples (Tang et al., 2013b; Zhou et al., 2008), which suggests that pyroxene is less susceptible to hydrothermal alteration than whole rocks, especially for Sm and Nd isotopes, and is an ideal mineral for insight into magmatism.

5.1. The modes of occurrence of the volatiles

The volatiles extracted from the Zhubu silicate minerals at the 200–400 °C, 400–900 °C and 900–1200 °C intervals could have intrinsically come from the different modes of occurrence, such as different stage of fluid inclusions, and crystal defects and site vacancies (Zhang et al., 2007, 2009, 2013a). These were trapped in different magmatic stages, and their volatiles have different chemical and carbon isotopic compositions. The chemical and isotopic variation of volatiles with extraction temperature could be related to the different modes of occurrence with different origins.

The volatiles released at the 200–400 °C interval show low contents and are composed of dominant H_2O (av. 507.57 $mm^3 \cdot STP/g$), and minor amounts of CO_2, C_2H_6 and N_2. These volatiles are interpreted to have derived from post-magmatic fluid inclusions (Zhang et al., 2009; Tang et al., 2013a). The significantly low $\delta^{13}C_{CO2}$ and $\delta^{13}C_{CH4}$ values for these volatiles are plotted into the ranges of crust origin and methane oxidation in the $\delta^{13}C_{CO2}$ and $\delta^{13}C_{CH4}$ diagram (Fig. 4a, Ueno et al., 2006), which indicates that these volatiles mainly originated from the crust and air-saturated fluids (Zhang et al., 2009, 2013a).

The volatiles in the primary silicate minerals of the Zhubu intrusion were mainly released at the 400–900 °C interval, showing high content and dominant H_2O (av. 9393.78 $mm^3 \cdot STP/g$) plus minor amounts of H_2 (av. 400.51 $mm^3 \cdot STP/g$) and CO_2 (av. 186.28 $mm^3 \cdot STP/g$). Lower amounts of volatiles were released at the 900–1200 °C interval including H_2O, CO_2 and SO_2 (av. 2376.07, 35.99 and 26.28 $mm^3 \cdot STP/g$, respectively).

H_2O, CO_2 and H_2 are released predominantly at the 400–900 °C interval. These volatiles are interpreted to have derived from fluid inclusions and OH^- in the crystal lattices of pyroxene, i.e., nominally anhydrous minerals (NAMs). SO_2 was mainly released at 900–1200 °C, and is interpreted to have derived from the decomposition of sulfide inclusions (Tang et al., 2013a). The volatiles released at the 400–900 °C and 900–1200 °C intervals could have derived from primary fluid inclusions, crystal structures and defects (Zhang et al., 2009), and are therefore interpreted to represent magmatic volatiles.

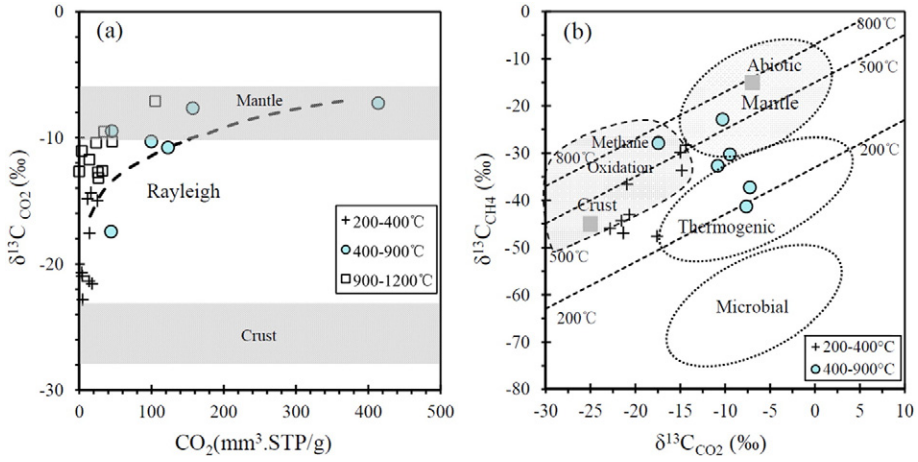

Fig. 4. Plots of $\delta^{13}C_{CO2}$ values (‰ v-PDB) versus the CO_2 contents (a) and $\delta^{13}C_{CH4}$ values (‰ v-PDB) (b, after Ueno et al., 2006) in the Zhubu intrusion. Rayleigh-Rayleigh degassing model of carbon isotopes (initial value of $\delta^{13}C_{CO2}$ is −7‰, 1000 lnα = 2.5‰).

Table 4
The Sr-Nd isotopic compositions of pyroxene separates in the Zhubu mafic-ultramafic intrusion.

Sample	Rock type	Rb (ppm)	Sr (ppm)	$^{87}Rb/^{86}Sr$	$^{87}Sr/^{86}Sr$	2σ	Sm (ppm)	Nd (ppm)	$^{147}Sm/^{144}Nd$	$^{143}Nd/^{144}Nd$	2σ	$(^{87}Sr/^{86}Sr)_i$	ε_{Nd} (t = 260 Ma)
ZB11-10	Lherzolite	1.76	50.38	0.101341	0.708497	0.000628	2.11	8.96	0.142055	0.512583	0.000828	0.708122	0.7
ZB11-11	Lherzolite	1.17	49.38	0.068347	0.708375	0.000717	1.87	7.59	0.149317	0.512521	0.000637	0.708122	−0.7
ZB11-14	Lherzolite	2.31	57.94	0.115147	0.708903	0.001305	2.01	9.08	0.133982	0.512507	0.001426	0.708477	−0.5
ZB11-16	Ol-Gabbro	13.66	110.20	0.358634	0.710238	0.000452	3.48	14.10	0.149255	0.512411	0.000930	0.708912	−2.8
ZB11-21	Ol-Gabbro	70.94	132.24	1.552599	0.712387	0.000923	7.58	36.21	0.126573	0.512396	0.000467	0.706644	−2.4
ZB11-22	Gabbro	43.72	329.94	0.383375	0.708730	0.000810	8.32	40.48	0.124239	0.512476	0.002006	0.707312	−0.8
ZB11-23	Gabbrodiorite	76.45	328.46	0.673377	0.708373	0.000799	8.91	42.86	0.125722	0.512507	0.001511	0.705882	−0.2

5.2. The compositions and origins of magmatic volatiles

5.2.1. The compositions of magmatic volatiles

The magmatic volatiles in Zhubu intrusion, as represented by the volatiles released from the primary silicate minerals at the 400–900 °C and 900–1200 °C intervals, are characterized by dominant H_2O (av. 11,649.6 $mm^3 \cdot STP/g$) and high contents of H_2 and CO_2 (av. 394.8 and 202.1 $mm^3 \cdot STP/g$, respectively). They have higher volatile contents than the volatiles in the silicate minerals of the Noril'sk Ni-Cu-PGE sulfide deposits in the Siberian LIP (Tang et al., 2013a) and the Fe-Ti-V oxide deposits in the Emeishan LIP (Xing et al., 2012), but they all show similar chemical compositions. The volatiles in the Noril'sk Ni-Cu-PGE sulfide deposits in the Siberian LIP are dominated by H_2O (av. 2286.0 $mm^3 \cdot STP/g$), and minor amounts of H_2, H_2S, CO_2 and SO_2 (av. 152.06, 93.27, 87.05 and 58.18 $mm^3 \cdot STP/g$, respectively) (Tang et al., 2013a). The volatiles of the Fe-Ti-V oxide deposits in the Emeishan LIP are also dominated by H_2O (av. 169.73 $mm^3 \cdot STP/g$), and minor amounts of H_2, H_2S and CO_2 (av. 112.81, 18.66 and 13.10 $mm^3 \cdot STP/g$, respectively) (Xing et al., 2012). In contrast, the magmatic volatiles in Zhubu intrusion are dramatically different in chemical compositions from the volatiles in the associated magnetite of the Fe-Ti-V oxide deposits which are dominated by SO_2 and CO_2 (av. 652.60 and 216.92 $mm^3 \cdot STP/g$, respectively) (Xing et al., 2012).

The volatiles in the magma system show behaviors similar to those of incompatible elements. The CO_2 will partition preferentially into exsolved vapor phase during the magma rising and cooling due to lower solubility in melt than H_2O (Lowenstern et al., 1991). Therefore, H_2O becomes concentrated in the residual melt during *in situ* fractional crystallization of vapor-saturated magma, but CO_2 is preferentially lost into the vapor phase, which can result in degassing of CO_2 without significant loss of H_2O (Dixon and Stolper, 1995; Wallace, 2005). A positive correlation between $\delta^{13}C_{CO2}$ values and CO_2 contents (Fig. 4a) can be caused by kinetic fractionation of carbon isotope by degassing, but it does not match the Rayleigh model of carbon isotope fractionation (Fig. 4a). Therefore, it suggests the existence of crustal contamination. This can mean that H_2O can be concentrated and trapped in the minerals from melt, but CO_2 and other volatiles are lost with the vapor degassing during rising and crystallization through the Zhubu magma conduit.

The original H_2O and CO_2 contents in mantle-derived magma may be estimated by the contents of Ce (Dixon and Clague, 2001) and Nb (Saal et al., 2002), respectively. H_2O contents in olivine from lherzolite with highest Nb/U value can represent the H_2O contents of parental magma, because this type of olivine is a mineral that crystallizes early on liquids with less crustal contamination. The H_2O content of the Zhubu parental magma is measured as 20,684.21 $mm^3 \cdot STP/g$ (i.e., 1.66 wt%) by the H_2O released at the 400–1200 °C interval from olivine separate of lherzolite (Nb/U = 21.35) in the Zhubu intrusion. It is higher than the estimated values (0.2–0.7 wt%) for basaltic magma of the Emeishan LIP (Ganino et al., 2008) and significantly higher than the H_2O contents (0.03–0.1 wt%) for the typical oceanic island basalts (Dixon and Clague, 2001; Hauri, 2002; Saal et al., 2002), indicating that the parental magma of the Zhubu intrusion was more H_2O-rich than the Emeishan basalts as well as typical oceanic island basalts.

The measured CO_2 content (428.05 $mm^3 \cdot STP/g$, i.e., 840 ppm) in the Zhubu magma is significantly lower than the values for the Emeishan basalts (2294–13,508 ppm) estimated by the Nb contents in the basalts (Xiao et al., 2004; Zhang et al., 2006), but it is within the range of CO_2 contents (120–1830 ppm) in the oceanic island basalts (Hirschmann and Dasgupta, 2009).

The primary silicate mineral separates have high H_2 contents in both magmatic Fe-Ti-V oxide deposits and Ni-Cu sulfide deposits in the

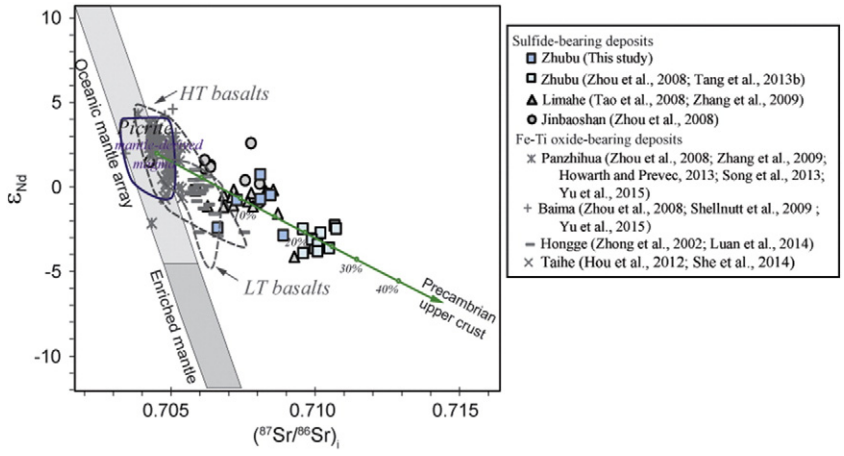

Fig. 5. Plot of ε_{Nd} (t = 260 Ma) vs. $(^{87}Sr/^{86}Sr)_i$ for the Zhubu intrusion. The mantle array is from Zindler and Hart (1986). The field for the Emeishan picrites is based on data from Chung and Jahn (1995), Hou et al. (2012), Li et al. (2012), Xu et al. (2001) and Zhang et al. (2006, 2008). The fields for the Emeishan high-Ti (HT) and low-Ti (LT) basalts are based on the data from Xu et al. (2001), Xiao et al. (2004) and Zhang et al. (2008). Values used in the mixing calculations: mantle-derived magma, 130 ppm Sr, 10.5 ppm Nd, $(^{87}Sr/^{86}Sr)_i$, 0.7045, ε_{Nd}, 2; upper crust, 320 ppm Sr, 27 ppm Nd, $(^{87}Sr/^{86}Sr)_i$, 0.718, ε_{Nd}, −10. The Sr and Nd contents in the crust are from Rudnick and Gao (2014). The Sr and Nd isotopes in the crust are from Chen and Jahn (1998).

Table 5
The Lu–Hf isotopes of zircons from gabbro in the Zhubu intrusion.

Analysis	Age (Ma)	$^{176}Yb/^{177}Hf$	2σ	$^{176}Lu/^{177}Hf$	2σ	$^{176}Hf/^{177}Hf$	2σ	$(^{176}Hf/^{177}Hf)_i$	$\varepsilon_{Hf}(t)$	T_{DM} (Ma)
ZB11-19-01	260.4	0.049817	0.000524	0.001185	0.000015	0.282631	0.000021	0.282625	0.53	884.3
ZB11-19-02	254.9	0.052890	0.000983	0.001172	0.000013	0.282636	0.000025	0.282630	0.59	877.3
ZB11-19-03	270.5	0.058963	0.001418	0.001415	0.000021	0.282601	0.000021	0.282594	−0.35	932.3
ZB11-19-04	259.6	0.054810	0.000465	0.001271	0.000004	0.282572	0.000022	0.282566	−1.60	970.6
ZB11-19-05	268.1	0.079120	0.002569	0.001746	0.000046	0.282646	0.000027	0.282637	1.12	876.4
ZB11-19-06	269.8	0.087751	0.001371	0.001931	0.000019	0.282528	0.000026	0.282518	−3.05	1051.0
ZB11-19-08	268.2	0.069507	0.000497	0.001544	0.000003	0.282597	0.000027	0.282589	−0.58	941.7
ZB11-19-22	268.5	0.042916	0.000162	0.001124	0.000004	0.282665	0.000026	0.282659	1.90	835.3

ε_{Hf} at the age of zircon crystallization was calculated using CHUR values of Blichert-Toft and Albarède (1997) and ^{176}Lu decay constant of Scherer et al. (2001).
T_{DM} was calculated from present-day depleted mantle values of $(^{176}Hf/^{177}Hf)_{DM} = 0.28325$ and $(^{176}Lu/^{177}Hf)_{DM} = 0.0384$ (Griffin et al., 2000).

Emeishan LIP and the Siberian LIP (Tang et al., 2013a), as well as the Kalatongke sulfide deposit in the Central Asian Orogenic Belt, China (Fu et al., 2012). This implies a reduced condition for these magmatic systems, because H is present only under reduced conditions and can be incorporated as OH^- into the crystal structure of pyroxene (e.g., Skogby and Rossman, 1989).

The most of large ore-bodies of Ni-Cu-PGE sulfide deposits always form in the magmatic conduit system or the chamber of *in situ* fractional crystallization during magma rising and evolution (Li et al., 2009). As suggested previously, the Zhubu intrusion was formed in two stages: an early conduit stage for the marginal zone and a late *in situ* differentiation stage for the layered sequence (Tang et al., 2013b). There are some differences in the chemical compositions of volatiles between the marginal zone and layered sequence. The volatiles released at the 400–1200 °C interval from the marginal zone have significantly higher H_2O contents (av. 14,669.48 $mm^3 \cdot STP/g$) and lower H_2, CO_2, H_2S and SO_2 (av. 238.45, 183.16, 30.04 and 8.72 $mm^3 \cdot STP/g$, respectively) contents than those from the layered sequence (av. 7420 H_2O, 657.36 H_2, 280.94 CO_2, 96.92 H_2S and 56.32 $mm^3 \cdot STP/g$ SO_2). The differences between the marginal zone and layered sequence cannot be interpreted by bake-degassing of magma, perhaps reflecting different volatile compositions in the different pulses of magma.

5.2.2. The origins of magmatic volatiles

A large amount of H_2O, as well as H_2, CO_2 and H_2S etc. in the Zhubu magma may have been derived from source mantle or crustal fluids. The $\delta^{13}C_{CO2}$ and $\delta^{13}C_{CH4}$ values for the volatiles released at the 400–900 °C interval plot between mantle and thermogenic origins (Fig. 4a, Deines, 2002), indicating that mantle-derived CO_2 and CH_4 were contaminated by the thermogenic components from sedimentary organic matters in the Zhubu magma (Fig. 4a). Carbon-rich external fluids with low $\delta^{13}C_{CO2}$ values could also be involved. The thermogenic crustal fluids could be from the degassing of country rocks. This fact is similar to the magnetite ores in Fe-Ti-V oxide-bearing mafic intrusions in the Emeishan LIP, where the volatiles could be derived from country rocks (Xing et al., 2012; Ganino et al., 2013).

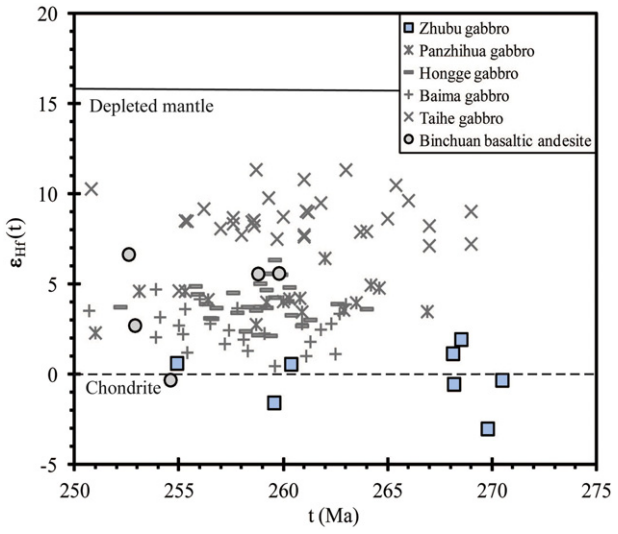

Fig. 6. Plot of zircon $\varepsilon_{Hf}(t)$ versus $^{206}Pb/^{238}U$ age (Ma) for different types of rocks in the Emeishan LIP. The data are from this study and references of Shellnutt et al. (2009), Zhong et al. (2009, 2011) and Tang et al. (2015).

The $(Nb/Th)_N$ and Nb/U ratios are good indicators of crustal assimilation, because they decrease with increasing contamination by siliceous crustal materials. The H_2 and H_2S contents in the volatiles from the Zhubu primary silicate minerals show the negative correlations with the whole rock $(Nb/Th)_N$ ratios (Fig. 7a, b). The $\delta^{13}C_{CO2}$ values at the 400–900 °C interval have a week negative correlation with whole rock $(Nb/Th)_N$ ratios (Fig. 7c), indicating the addition of external CO_2 to the magma by the crustal assimilation. The H_2/N_2 ratios show a negative correlation with whole rock Nb/U ratios (Fig. 7d), suggesting the addition of external H_2 and H_2S to the magma by the assimilation of crustal material as well.

The variation of volatile contents in the pyroxene of different types of rocks in the marginal zone and layered sequence may be related to variable sources of volatiles. The volatiles released at the 400–900 °C interval from pyroxene separates from the marginal zone show that the H_2O contents decrease significantly from lherzolite (av., 13,107 $mm^3 \cdot STP/g$) to olivine websterite (4143 $mm^3 \cdot STP/g$), and that the CO_2 contents increase conversely from lherzolite (103 $mm^3 \cdot STP/g$) to olivine websterite (414 $mm^3 \cdot STP/g$). These are consistent with separate pulses of magma for the different units. In contrast, the H_2O and CO_2 contents in the volatiles released at the 400–900 °C interval from the pyroxene separates from the layered sequence increase from olivine gabbro (av., 3181 and 101 $mm^3 \cdot STP/g$, respectively) to gabbro (5676 and 157 $mm^3 \cdot STP/g$) and to gabbrodiorite (13,106 and 604 $mm^3 \cdot STP/g$), which are consistent with magma differentiation of a single pulse. This scenario is supported by petro-geochemical evidence that the layered sequence in the Zhubu intrusion was formed by *in situ* fractional crystallization of a pulse of magma (Tang et al., 2013b).

5.3. Mantle source variation, fertile magma and sulfide mineralization

Magma fertile in chalcophile elements (such as Ni, Cu and PGE) and sulfur saturation in the magma system during magma formation and evolution are two critical factors in the formation of magmatic Cu-Ni-PGE sulfide deposits.

5.3.1. Source mantle characteristics

5.3.1.1. A H_2O-rich source mantle for Zhubu magma. The Nd isotopic compositions of pyroxene separates from the Zhubu intrusion overlap the ranges for the coeval flood basalts (both high-Ti and low-Ti), picrites and other magmatic Ni-Cu-PGE sulfide-bearing mafic-ultramafic intrusions in the Emeishan LIP (Fig. 5). Moreover, the ε_{Nd} and ε_{Hf} values for

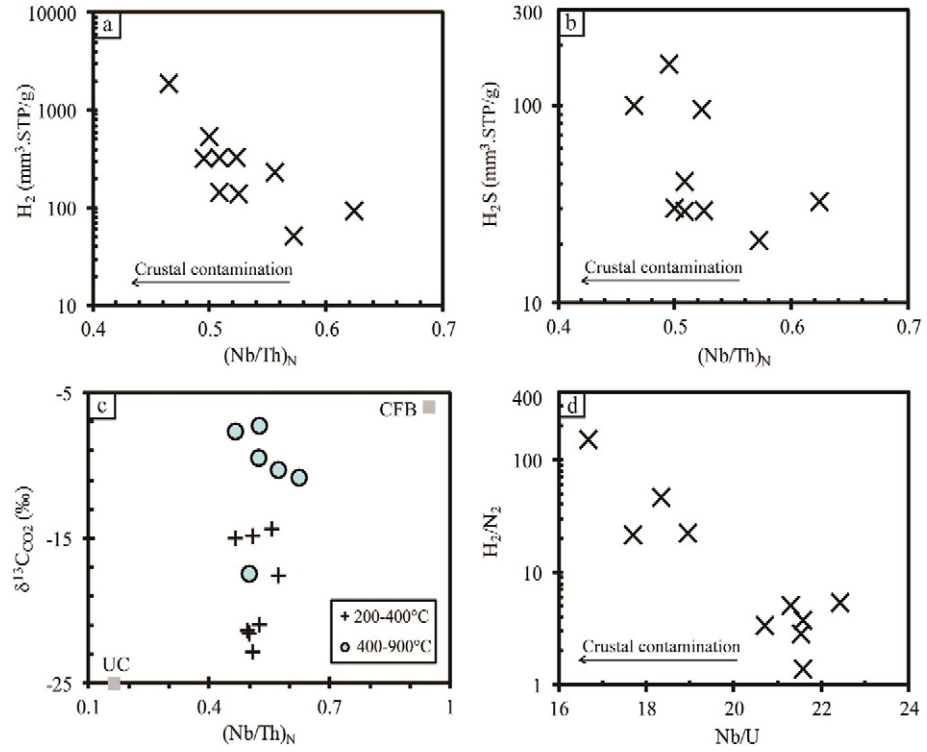

Fig. 7. Plots of $(Nb/Th)_N$ versus H_2 (a) and H_2S (b) contents and $\delta^{13}C_{CO2}$ (c), and H_2/N_2 versus Nb/U (d) in the Zhubu intrusion. The Nb, Th and U contents of the Zhubu samples are from Tang et al. (2013b). The average composition of continental flood basalts (CFBs) is from Li et al. (2015). The composition of the upper crust (UC) is from Rudnick and Gao (2014). The primitive mantle values for normalization are from Palme and O'Neill (2014). The $\delta^{13}C_{CO2}$ of the CFB and UC are from Deines (2002).

the Zhubu intrusion are within the ranges for mantle plume-related basalts in oceanic island and plateau settings (Fig. 8, Salters et al., 2011). These geochemical similarities indicate that the magma of the Zhubu intrusion generally shares a common source mantle with the coeval flood basalts that are widely accepted as the products of mantle plume activity in the Permian (Wang et al., 2006, 2007; Zhou et al., 2008; Liao et al., 2015).

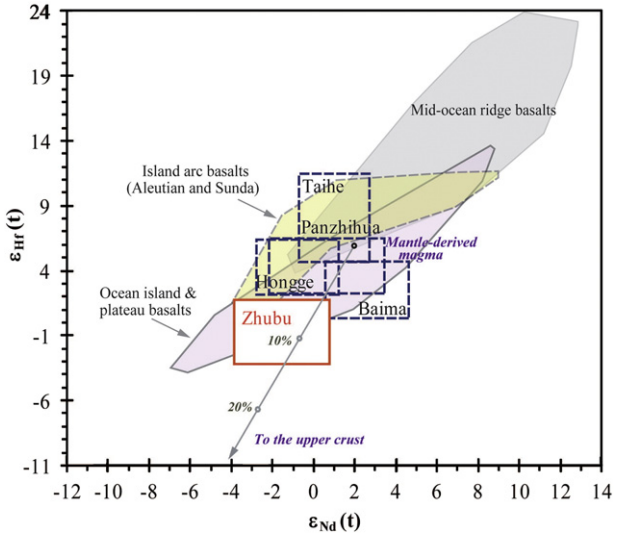

Fig. 8. Plot of zircon $\varepsilon_{Hf}(t)$ versus whole-rock $\varepsilon_{Nd}(t)$ for the Zhubu mafic-ultramafic intrusion. Data sources: Zhubu gabbro (this study, Tang et al., 2013b); Panzhihua gabbro (Zhong et al., 2011; Zhou et al., 2005, 2008; Zhang et al., 2009; Howarth and Prevec, 2013); Baima gabbro (Zhong et al., 2011; Shellnutt et al., 2009; Zhou et al., 2008); Hongge gabbro (Zhong et al., 2009, 2011); Taihe gabbro (Zhong et al., 2011; Shellnutt et al., 2011; Hou et al., 2012); Aleutian and Sunda arcs (Handley et al., 2011; Yogodzinski et al., 2010); and mid-ocean ridge basalts and ocean island-plateau basalts (Salters et al., 2011).

The distinctive trace elemental and isotopic compositions between sulfide- and oxide-bearing intrusions in the Emeishan LIP imply source mantle heterogeneity (Zhou et al., 2008; Zhang et al., 2009) or different degrees of lithospheric materials or crustal contamination (Shellnutt et al., 2011). The source mantle heterogeneity is also suggested by large variation of *syn*-magmatic zircon $\varepsilon_{Hf}(t)$ values in the Emeishan LIP, because the zircon derived from a homogenous source would not yield considerable varying $\varepsilon_{Hf}(t)$ values. The Zhubu intrusion has lower zircon ε_{Hf} and whole rock ε_{Nd}, and slightly higher whole rock $(^{87}Sr/^{86}Sr)_i$ than the coeval Fe-Ti-V oxide-bearing mafic intrusions and basaltic andesite in the Emeishan LIP (Fig. 8) (Shellnutt et al., 2011; Zhong et al., 2011). The mixing calculation shows that the Zhubu parental magma before crustal contamination has a slightly lower ε_{Nd} value (approximately 2, Fig. 5) than the coeval mafic intrusions that host Fe-Ti-V oxide deposits, indicating a more enriched source mantle for the Zhubu intrusion than that for the other intrusions (Figs. 5, 8).

Some researchers (e.g., Zhou et al., 2008) have suggested that the magmatic Cu–Ni–PGE sulfide-bearing and the coeval magmatic V–Ti–Fe oxide-bearing intrusions in the Emeishan LIP are different in their magma series and source mantle isotope compositions. The parental magma for the Zhubu intrusion is inferred to have higher H_2O contents than the coeval magmatic V–Ti–Fe oxide-bearing intrusions in Emeishan LIP based on volatile compositions; it may also be related to higher H_2O content in the source mantle for the Zhubu intrusion than that for the V–Ti–Fe oxide-bearing intrusions.

5.3.1.2. The roles of CO_2–rich fluid and water. High abundances of chalcophile elements such as Ni, Cu and PGE in ore-forming magma are important for the formation of magmatic Ni-Cu-PGE sulfide deposits, and can be generated and assembled by high degree of partial melting in the mantle (Naldrett, 1999). The inferred high H_2O content in source mantle for the Zhubu intrusion could increase the degree of partial melting in the mantle, thereby producing a chalcophile element fertile parental magma for the deposit, because H_2O can lower the temperature of initial partial melting. High-degree partial melts are

enriched in Ni due to melting of abundant olivine, which is the major host of Ni in the mantle. High-degree partial melts are also enriched in other chalcophile elements, such as Cu and PGE, because no sulfide or platinum-group mineral (PGM) is left behind. The melting of sulfide in the source mantle will transfer sulfur from the mantle to the partial melt, producing sulfur-bearing magmas, such as the olivine-hosted melt inclusions containing 1311 ppm S in the Emeishan picrites (Zhang et al., 2013b).

Alternatively, as indicated by experiments, the chalcophile elements could be transported and added to a mantle-derived magma by supercritical CO_2–rich fluids under mantle conditions (Blackburn et al., 2001). The observed positive correlation between the whole rock Cu and Ni contents and the CO_2 contents in the mineral separates in the Kalatongke magmatic sulfide deposit (Fu et al., 2012) may be related to CO_2 transportation of these metals. The positive correlations between H_2O and H_2S contents at 400–900 °C from pyroxene separates and the whole rock Pt and Pd contents from the Zhubu deposit are also consistent with volatile transportation of these metals (Fig. 9).

5.3.2. Sulfide saturation

Sulfide saturation in mafic magma and sulfide-liquid accumulation in limited localities in dynamic magmatic systems are critical for the formation of Cu-Ni-PGE sulfide deposit. Sulfide saturation may be caused by the addition of H_2S and H_2 (a reduced gas) and crustal contamination (Tang et al., 2013b). The addition of external sulfur from the S-rich country rocks is perhaps the most effective way of causing sulfide saturation in magma. This process is thought to have played a critical role in the formation of many world-class magmatic Ni-Cu-PGE sulfide deposits, such as the Noril'sk-Talnakh deposits in the Siberia LIP (e.g. Arndt et al., 2003; Li et al., 2003, 2016).

5.3.2.1. Addition of S and reduced gas.. The sulfur content at sulfide saturation (SCSS) of an H_2O-bearing mafic magma may be much lower than its anhydrous counterpart (Ripley and Li, 2013). Our data show that the primary silicate mineral separates from the marginal zone of the Zhubu intrusion contain significantly higher H_2O (av. 11,612.79 $mm^3 \cdot STP/g$) and lower H_2S (av. 30.04) and SO_2 (av. 8.7) than the layered sequence (av. 6065.25, 96.9 and 56.3 $mm^3 \cdot STP/g$ for H_2O, H_2S and SO_2, respectively). We attribute the lower abundances of S-bearing volatiles in the marginal zone to sulfide saturation and segregation prior to the crystallization of the silicate minerals from the magma of the marginal zone.

The sulfur contents (av. 87.73 $mm^3 \cdot STP/g$, i.e., 125 ppm) in the primary silicate mineral separates from the Zhubu intrusion are higher than the sulfur content (83 ppm) for the typical mantle plume (Tang et al., 2013b; Zhang et al., 2013b), but are significantly lower than the sulfur content (1311 ppm) in the olivine-hosted melt inclusions in the Emeishan picrites from Dali (Zhang et al., 2013b). We speculate that the low H_2S and SO_2 contents (av. 59.8 and 27.8 $mm^3 \cdot STP/g$, respectively) in the mineral separates from the Zhubu intrusion are due to previous sulfide segregation at its deep process. Olivine separates from the marginal zone of the Zhubu intrusion have lower H_2S contents (av. 41.1 $mm^3 \cdot STP/g$) than other silicate minerals, consistent with sulfide segregation before olivine crystallization in the Zhubu magmatic system (Tang et al., 2013b).

The positive correlation between H_2S contents in mineral separates and the estimated degrees of crustal contamination for whole rocks (Fig. 7b) indicate that crustal sulfur was involved in the magmatic process. The amounts of H_2S and SO_2 released from pyroxene separates at the 400–900 °C interval increase from lherzolite (av. 24.2 and 8.2 $mm^3 \cdot STP/g$, respectively), to olivine websterite (30.7 and 11.3), to olivine gabbro (97.2 and 36.4) and to gabbro (160.9 and 119.2) (Table 1), consistent with the addition of sulfur-bearing fluids into the magma during crystallization. The thermogenic $\delta^{13}C$ of volatile in the Zhubu minerals imply that the sulfur-rich fluids could be from country rocks (Fig. 4b).

The primary mineral separates from the Zhubu intrusion have high H_2 contents, perhaps due to a reduced parental magma. The maximum S solubility in a reduced magma where sulfide is stable is approximately one order of magnitude lower than that in an oxidized magma where

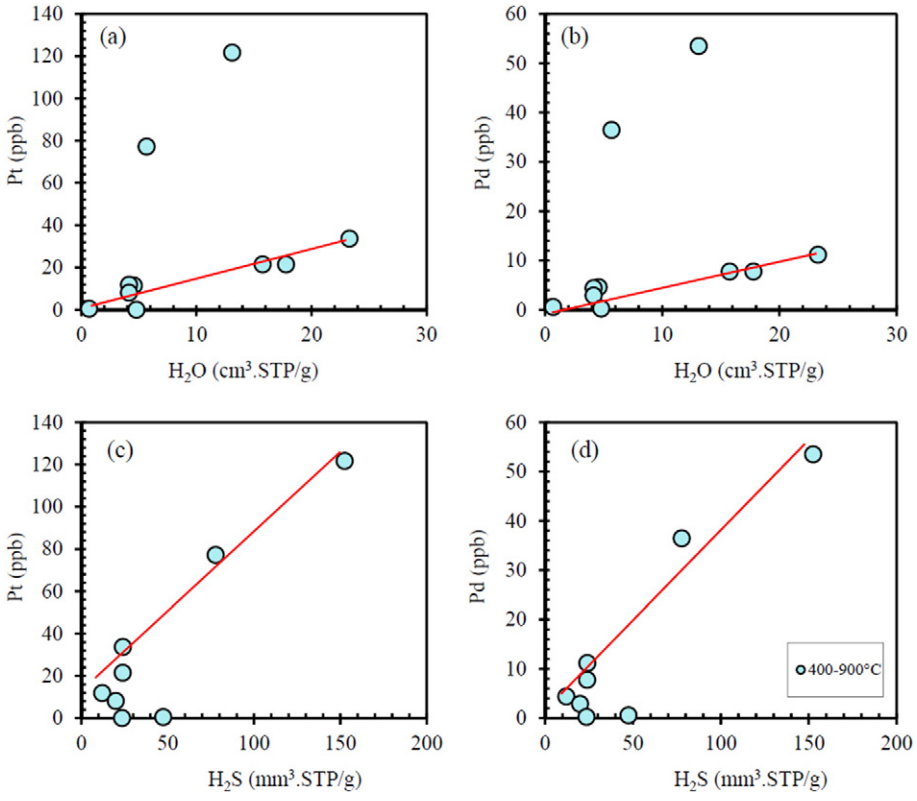

Fig. 9. The H_2O (a, b) and H_2S (c, d) contents in pyroxene correlated with the whole rock Pd and Pt concentrations in the Zhubu intrusion. The Pd and Pt data are from Tang et al., 2013b.

sulfate is stable (e.g., Jugo et al., 2005). The negative correlation between the CO_2 contents and H_2/CO_2 ratios and the positive correlation between the H_2/CH_4 ratios and $\delta^{13}C_{CO2}$ values for the volatiles at the 400–900 °C interval from silicate mineral separates are present in the Zhubu sulfide deposit as well as the coeval Fe-Ti-V oxide deposits in the Emeishan LIP (Xing et al., 2012) (Fig. 10). However, the Zhubu deposit is characterized by higher H_2/CO_2 and H_2/CH_4 ratios than the Fe-Ti-V oxide deposits (Fig. 10), indicating a more reduced condition for the Zhubu deposit than the Fe-Ti-V oxide deposits in the Emeishan LIP. A more reduced condition results in low maximum S solubility, and is easy to trigger sulfide saturation for the Zhubu deposit (Jugo et al., 2005).

5.3.2.2. Crustal contamination. Sulfide saturation in the Zhubu magma could also be triggered by crustal contamination, as indicated by the whole rock trace elements (Tang et al., 2013b) and integrated C-Sr-Nd-Hf isotopes. The addition of H_2 and H_2S to the magma could occur together with siliceous crustal contamination, triggering faster sulfide saturation in the magma.

The Sr-Nd isotopic compositions of pyroxene separates from the Zhubu intrusion indicate ~15 wt% assimilation of the upper crust in a mantle-derived magma with an initial ε_{Nd} value of ~2 (Fig. 5). Previous whole rock Sr-Nd isotopic data indicate higher degrees of crustal contamination between 25 and 35 wt% (Tang et al., 2013b). The negative ε_{Hf} values for gabbro zircon crystals from the Zhubu intrusion are consistent with significant crustal contamination. Based on a maximum of 15 wt% crustal contamination constrained by pyroxene Sr-Nd isotopes and the observed ε_{Hf} values for zircon from the Zhubu gabbro, the estimated initial ε_{Hf} values for the parental magma of the Zhubu gabbro is 5.9. This value is lower than those for the parental magmas of the coeval Fe-Ti-V oxide deposits in the Emeishan LIP, indicating that the source mantle of the Zhubu intrusion is more enriched isotopically than that of the coeval Fe-Ti-V oxide deposits (Fig. 8).

The integrated C-Sr-Nd isotopes show highly variable crustal contamination in the Zhubu intrusion from 5 to 30 wt% (Fig. 11). The $\delta^{13}C_{CO2}$ of the silicate mineral separates from the Zhubu intrusion are significantly lower than the $\delta^{13}C_{CO2}$ values of the coeval Panzhihua and Baima Fe-Ti-V oxide ore-bearing intrusions, but they are slightly higher than the values of the Hongge mafic intrusion, which hosts a major Fe-Ti-V oxide deposit and extensive sulfide mineralization (Xing et al., 2012). Such regional variation is consistent with increasing crustal contamination from Panzhihua-Baima to Zhubu-Hongge (Ganino et al., 2013; Yu et al., 2015). Based on Sr-Nd-Hf isotopic compositions, the contaminants of the magmas of the Fe-Ti-V oxide ore-bearing intrusions were thought to have derived from the continental middle crust (Zhou et al., 2008). The Sr-Nd-Hf isotope data for the Zhubu intrusion are more consistent with contamination by the continental upper crust (Fig. 5).

The single stage Hf model ages (835 Ma–1051 Ma) of zircon crystals from Zhubu intrusion are significantly older than the crystallization age of the Zhubu magma, indicating that the Zhubu magma experienced significant crustal contamination, or was derived from a highly enriched mantle. The C, Nd and Hf isotopes together are more consistent with the crustal contamination. Mixing calculation shows that the Neoproterozoic crustal materials in the region are the best candidates for the contaminants. Carbon isotopes support crustal contamination from sedimentary organic matters of country rock (Fig. 4b). The $\delta^{13}C$ values of the CO_2 and CH_4 released at the 400–900 °C intervals from the primary silicate minerals from the Zhubu intrusion are consistent with the interpretation that the Zhubu magma was contaminated by carbon-rich fluids containing thermogenic components, which could be derived from the sedimentary rocks (Fig. 4).

6. Conclusions

(1) Zircon crystals from the layered sequence of the Zhubu mafic-ultramafic intrusion yield a mean $^{206}Pb/^{238}U$ age of 263.2 ± 5.6 Ma, which confirms that the Zhubu intrusion is a part of the Permian Emeishan LIP. The volatiles extracted at high temperatures from the primary silicate mineral separates in the Zhubu intrusion are dominated by H_2O, with minor H_2 and CO_2, indicating a reduced condition and a H_2O-rich parental magma. The layered sequence is characterized by lower H_2O, and higher H_2, CO_2, H_2S and SO_2 contents in the mineral separates than the marginal zone, which is consistent with different pulses of magma with different volatile compositions.

(2) The Sr-Nd-Hf isotopic compositions of the Zhubu intrusion indicate ~15 wt% contamination with the upper crust in a mantle-derived magma with initial ε_{Nd} value close to 2. The carbon isotopes of volatiles at high temperatures indicate that the thermogenic components of sedimentary country rocks were added to the Zhubu magma.

(3) The integrated C-Sr-Nd-Hf isotopes ($(^{87}Sr/^{86}Sr)_i = 0.705882$–$0.708912$; $\varepsilon_{Nd} = -2.8$–0.7; $\varepsilon_{Hf} = -3.05$–$+1.90$) indicate that there are differences in the source mantle compositions as well as contamination materials between the Zhubu intrusion and some coeval Fe-Ti-V oxide-bearing intrusions in the Emeishan LIP. The sulfide saturation in the Zhubu magma was triggered by crustal contamination including the addition of volatiles.

Supplementary data to this article can be found online at http://dx.doi.org/10.1016/j.chemgeo.2017.02.009.

Acknowledgements

This study was financially supported by the Special Fund for the Land and Resources Scientific Research of Public Interest (201511020), the NSF of China (41472070, 41372095), the Spec. Fund for the Doctoral Program of Higher Education (20120211110023), Key Project of Ministry of Education of the People's Republic of China (311010), the

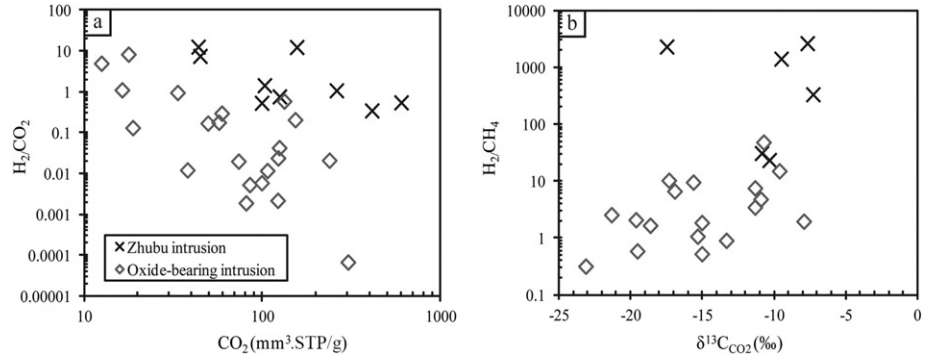

Fig. 10. The plots of CO_2 contents versus H_2/CO_2 ratios (a) and H_2/CH_4 ratios versus $\delta^{13}C_{CO2}$ values (b) at the 400–900 °C interval in the Zhubu intrusion. Data for oxide-bearing intrusions are from Xing et al. (2012).

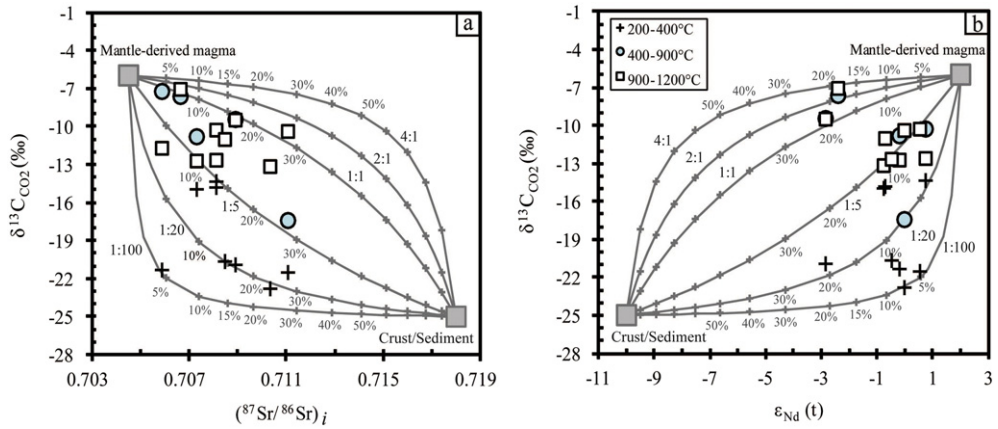

Fig. 11. Plots showing variations of $\delta^{13}C$ (‰ v-PDB) of CO_2 with $(^{87}Sr/^{86}Sr)_i$ (a) and ε_{Nd} (b) in the Zhubu intrusion. Values used in the mixing calculations: mantle-derived magma, 130 ppm Sr, 10.5 ppm Nd, $(^{87}Sr/^{86}Sr)_i$, 0.7045, ε_{Nd}, 2, $\delta^{13}C$, −6‰; Precambrian upper crust/subducted oceanic sediments, 320 ppm Sr, 27 ppm Nd, $(^{87}Sr/^{86}Sr)_i$, 0.718, ε_{Nd}, −10, $\delta^{13}C$, −25‰. The concentrations of Sr and Nd in the crusts are from Rudnick and Gao (2014). The Sr and Nd isotopes in the crusts are from Chen and Jahn (1998). The C isotopes in the mantle and crust are from Deines (2002). The mixing curves were constructed using different C_{Mantle}/C_{Crust} elemental ratios from 1:100 to 4:1.

Fundamental Research Funds for the Central Universities (lzujbky-2015-64) and the Fund of Gansu Key Lab of Mineral Resources in Western China (WCRMGS-2014-04). We gratefully thank Chusi Li for his great help in the manuscript revision, and Huaikun Li, Hongying Qiu, Kejun Hou, Yurong Cui, Chunhui Cao, Xieyan Song, Liwu Li, Piaoer Fu and Maochao Zhang for their assistance in the fieldwork, sampling and analysis.

References

Arndt, N.T., Czamanske, G.K., Walker, R.J., Chauvel, C., Fedorenko, V.A., 2003. Geochemistry and origin of the intrusive hosts of the Noril'sk-Talnakh Cu-Ni-PGE sulfide deposits. Econ. Geol. 98, 495–515.

Blackburn, J.M., Long, D.P., Cabanas, A., Watkins, J.J., 2001. Deposition of conformal copper and nickel films from supercritical carbon dioxide. Science 294, 141–145.

Blichert-Toft, J., Albarède, F., 1997. The Lu–Hf isotope geochemistry of chondrites and the evolution of the mantle–crust system. Earth Planet. Sci. Lett. 148, 243–258.

Chen, J., Jahn, B.M., 1998. Crustal evolution of southeastern China: Nd and Sr isotopic evidence. Tectonophysics 284, 101–133.

Chung, S.L., Jahn, B.M., 1995. Plume–lithosphere interaction in the generation of the Emeishan flood basalts at the Permian–Triassic boundary. Geology 23, 889–892.

Deines, P., 2002. The carbon isotope geochemistry of mantle xenoliths. Earth Sci. Rev. 58, 247–278.

Dixon, J.E., Clague, D.A., 2001. Volatiles in basaltic glasses from Loihi Seamount, Hawaii: evidence for a relatively dry plume component. J. Petrol. 42 (3), 627–654.

Dixon, J.E., Stolper, E.M., 1995. An experimental study of water and carbon dioxide solubilities in mid-ocean ridge basaltic liquids. Part II: applications to degassing. J. Petrol. 36, 1633–1646.

Fan, W., Zhang, C., Wang, Y., Guo, F., Peng, T., 2008. Geochronology and geochemistry of Permian basalts in Western Guangxi Province, Southwest China: evidence for plume-lithosphere interaction. Lithos 102, 218–236.

Fu, P., Tang, Q., Zhang, M., Zhang, Z., Li, L., Li, W., 2012. The ore genesis of Kalatongke Cu-Ni sulfide deposit, West China: constrains from volatile chemical and carbon isotopic compositions. Acta Geol. Sin.-English 86 (3), 568–578.

Ganino, C., Arndt, N.T., Zhou, M.F., Gaillard, F., Chauvel, C., 2008. Interaction of magma with sedimentary wall rock and magnetite ore genesis in the Panzhihua mafic intrusion, SW China. Miner. Deposita 43 (6), 677–694.

Ganino, C., Harris, C., Arndt, N.T., Prevec, S.A., Howarth, G.H., 2013. Assimilation of carbonate country rock by the parent magma of the Panzhihua Fe-Ti-V deposit (SW China): evidence from stable isotopes. Geosci. Front. 4, 547–554.

Griffin, W.L., Pearson, N.J., Belousova, E., Jackson, S.E., van Achterbergh, E., O'Reilly, S.Y., Shee, S.R., 2000. The Hf isotope composition of cratonic mantle: LAM-MC-ICPMS analysis of zircon megacrysts in kimberlites. Geochim. Cosmochim. Acta 64, 133–147.

Handley, H.K., Turner, S., Macpherson, C.G., Gertisser, R., Davidson, J.P., 2011. Hf–Nd isotope and trace element constraints on subduction inputs at island arcs: limitations of Hf anomalies as sediment input indicators. Earth Planet. Sci. Lett. 304, 212–223.

Hauri, E., 2002. SIMS analysis of volatiles in silicate glasses, 2: isotopes and abundances in Hawaiian melt inclusions. Chem. Geol. 183 (1), 115–141.

Hirschmann, M.M., Dasgupta, R., 2009. The H/C ratios of Earth's near-surface and deep reservoirs, and consequences for deep earth volatile cycles. Chem. Geol. 262, 4–16.

Hoskin, P.W.O., Schaltegger, U., 2003. The composition of zircon and igneous and metamorphic petrogenesis. In: Hanchar, J.M., Hoskin, P.W.O. (Eds.), Zircon. 53, pp. 27–62 (Rev. Mineral. Geochem.).

Hou, K.J., Li, Y.H., Tian, Y.Y., 2009. In situ U-Pb zircon dating using laser ablation-multi ion counting-ICP-MS. Mineral Deposits 28, 481–492 (in Chinese with English abstract).

Hou, T., Zhang, Z.C., Ye, X., Encarnacion, J., Reichow, M.K., 2011. Noble gas isotopic systematics of Fe-Ti-V oxide ore-related mafic-ultramafic layered intrusions in the Panxi area, China. Geochim. Cosmochim. Acta 75, 6727–6741.

Hou, T., Zhang, Z., Encarnacion, J., Santosh, M., 2012. Petrogenesis and metallogenesis of the Taihe gabbroic intrusion associated with Fe-Ti-oxide ores in the Panxi district, Emeishan Large Igneous Province, Southwest China. Ore Geol. Rev. 49, 109–127.

Howarth, G.H., Prevec, S.A., 2013. Trace element, PGE, and Sr–Nd isotope geochemistry of the Panzhihua mafic layered intrusion, SW China: constraints on ore-forming processes and evolution of parent magma at depth in a plumbing-system. Geochim. Cosmochim. Acta 120, 459–478.

Jugo, P.J., Luth, R.W., Richards, J.P., 2005. Experimental data on the speciation of sulfur as a function of oxygen fugacity in basaltic melts. Geochim. Cosmochim. Acta 69, 497–503.

Keays, R.R., Lightfoot, P.C., 2010. Crustal sulfur is required to form magmatic Ni-Cu sulfide deposits: evidence from chalcophile element signatures of Siberian and Deccan Trap basalts. Mineral. Deposita 45, 241–257.

Li, C., Ripley, E.M., Naldrett, A.J., 2003. Compositional variation of olivine and sulfur isotopes in the Noril'sk and Talnakh intrusions, Siberia: implications for ore-forming processes in dynamic magma conduits. Econ. Geol. 98, 69–86.

Li, C., Ripley, E.M., Naldrett, A.J., 2009. A new genetic model for the giant Ni-Cu-PGE sulfide deposits associated with the Siberian flood basalts. Econ. Geol. 104, 291–301.

Li, C., Tao, Y., Qi, L., Ripley, E.M., 2012. Controls on PGE fractionation in the Emeishan picrites and basalts: constraints from integrated lithophile-siderophile elements and Sr-Nd isotopes. Geochim. Cosmochim. Acta 90, 12–32.

Li, C., Arndt, N.T., Tang, Q., Ripley, E.M., 2015. Trace element indiscrimination diagrams. Lithos 232, 76–83.

Li, C., Ripley, E.M., Tao, Y., Hu, R., 2016. The significance of PGE variations with Sr-Nd isotopes and lithophile elements in the Emeishan flood basalt province from SW China to northern Vietnam. Lithos 248–251, 1–11.

Liao, M.Y., Tao, Y., Song, X.Y., Li, Y., Xiong, F., 2015. Multiple magma evolution and ore-forming processes of the Hongge layered intrusion, SW China. J. Asian Earth Sci. 113, 1082–1099.

Lowenstern, J.B., Mahood, G.A., Rivers, M.L., 1991. Evidence for extreme partitioning of copper into a magmatic vapor phase. Science 252, 1505–1509.

Ludwig, K.R., 2003. User's Manual for Isoplot 3.00: A Geolocronolgical Toolkit for Microsoft Excel. Berkeley Geochronological Center Special Publication, Berkeley (No. 4, 71pp).

Naldrett, A.J., 1999. World-class Ni-Cu-PGE deposits: key factors in their genesis. Mineral. Deposita 34 (3), 227–240.

Palme, H., O'Neill, H.S.C., 2014. Cosmochemical estimates of mantle composition. In: Richard, W.C. (Ed.), Treatise on Geochemistry. Elsevier, Amsterdam, pp. 1–38.

Revillon, S., Chauvel, C., Arndt, N.T., Pik, P., Martineau, F., Fourcade, S., Marty, B., 2002. Heterogeneity of the Caribbean plateau mantle: Sr, O and He isotopic compositions of olivine and clinopyroxene from Gorgona Island. Earth Planet. Sci. Lett. 205, 91–106.

Ripley, E.M., Li, C., 2013. Sulfide saturation in mafic magmas: is external sulfur required for magmatic Ni-Cu-(PGE) ore genesis? Econ. Geol. 108, 45–58.

Robertson, J., Ripley, E.M., Barnes, S.J., Li, C., 2015. Sulfur liberation from country rocks and incorporation in mafic magmas. Econ. Geol. 110, 1111–1123.

Rudnick, R.L., Gao, S., 2014. Composition of the continental crust. In: Rudnick, R.L. (Ed.), Treatise on Geochemistry. Elsevier, Amsterdam, pp. 1–51.

Saal, A.E., Hauri, E.H., Langmuir, C.H., Perfit, M.R., 2002. Vapour undersaturation in primitive mid-ocean-ridge basalt and the volatile content of Earth's upper mantle. Nature 419 (6906), 451–455.

Salters, V.J.M., Mallick, S., Hart, S.R., Langmuir, C.E., Stracke, A., 2011. Domains of depleted mantle: new evidence from hafnium and neodymium isotopes. Geochem. Geophys. Geosyst. 12:Q08001. http://dx.doi.org/10.1029/2011GC003617.

Scherer, E., Münker, C., Mezger, K., 2001. Calibration of the Lutetium-Hafnium Clock. Science 293, 683–687.

Shellnutt, J.G., Zhou, M.F., Zellmer, G.F., 2009. The role of Fe-Ti oxide crystallization in the formation of A-type granitoids with implications for the Daly gap. Chem. Geol. 259, 204–217.
Shellnutt, J.G., Wang, K.L., Zellmer, G.F., Iizuka, Y., Jahn, B.M., Pang, K.N., Qi, L., Zhou, M.F., 2011. Three Fe-Ti oxide ore-bearing gabbro-granitoid complexes in the Panxi region of the Permian Emeishan large igneous province, SW China. Am. J. Sci. 311, 773–812.
Shellnutt, J.G., Usuki, T., Kennedy, A.K., Chiu, H.Y., 2015. A lower crust origin of some flood basalts of the Emeishan large igneous province, SW China. J. Asian Earth Sci. 109, 74–85.
Skogby, H., Rossman, G.R., 1989. OH^- in pyroxene: an experimental study of incorporation mechanisms and stability. Am. Mineral. 74, 1059–1069.
Song, X.Y., Zhou, M.F., Hou, Z.Q., Cao, Z.M., Wang, Y.L., Li, Y., 2001. Geochemical constraints on the mantle source of the upper Permian Emeishan continental flood basalts, Southern China. Int. Geol. Rev. 43, 213–225.
Tang, Q., Zhang, M., Li, C., Yu, M., Li, L., 2013a. The chemical compositions and abundances of volatiles in the Siberian large igneous province: constraints on magmatic CO_2 and SO_2 emissions into the atmosphere. Chem. Geol. 339, 84–91.
Tang, Q., Ma, Y., Zhang, M., Li, C., Tao, Y., Zhu, D., 2013b. The origin of Ni-Cu-PGE sulfide mineralization in the margin of the Zhubu mafic-ultramafic intrusion in the Emeishan large igneous province, SW China. Econ. Geol. 108, 1889–1901.
Tang, Q., Li, C., Zhang, M., Ripley, E., Wang, Q., 2014. Detrital zircon constraint on the timing of amalgamation between Alxa and Ordos, with exploration implications for Jinchuan-type Ni–Cu ore deposit in China. Precambrian Res. 255, 748–755.
Tang, Q., Li, C., Zhang, M., Lin, Y., 2015. U–Pb age and Hf isotopes of zircon from basaltic andesite and geochemical fingerprinting of the associated picrites in the Emeishan large igneous province, SW China. Mineral. Petrol. 109, 103–114.
Ueno, Y., Yamada, K., Yoshida, N., Maruyama, S., Isozaki, Y., 2006. Evidence from fluid inclusions for microbial methanogenesis in the early Archaean era. Nature 440, 516–519.
Wallace, P.J., 2005. Volatiles in subduction zone magmas: concentrations and fluxes based on melt inclusions and volcanic gas data. J. Volcanol. Geotherm. Res. 140, 217–240.
Wang, C.Y., Zhou, M.F., Keays, R.R., 2006. Geochemical constraints on the origin of the Permian Baimazhai maficultramafic intrusion, SW China. Contrib. Mineral. Petrol. 152, 309–321.
Wang, C.Y., Zhou, M.F., Qi, L., 2007. Permian basalts and mafic intrusions in the Jinping (SW China)-Song Da (northern Vietnam) district: mantle sources, crustal contamination and sulfide segregation. Chem. Geol. 243, 317–343.
Wu, F.Y., Yang, Y.H., Xie, L.W., Yang, J.H., Xu, P., 2006. Hf isotopic compositions of the standard zircons and baddeleyites used in U–Pb geochronology. Chem. Geol. 234, 105–126.
Xiao, L., Xu, Y.G., Mei, H.J., Zheng, Y.F., He, B., 2004. Distinct mantle sources of low-Ti and high-Ti basalts from the western Emeishan large igneous province, SW China. Earth Planet. Sci. Lett. 228, 525–546.
Xing, C.M., Wang, C.Y., Zhang, M., 2012. Volatile and C-H-O isotopic compositions of giant Fe-Ti-V oxide deposits in the Panxi region and their implications for the source of volatiles and the origin of Fe-Ti oxide ores. Sci. China Earth Sci. 55, 1782–1795.
Xu, Y.G., Chung, S.-L., Jahn, B.-M., Wu, G., 2001. Petrologic and geochemical constraints on the petrogenesis of mian-Triassic Emeishan flood basalts in southwestern China. Lithos 58, 145–168.
Xu, Y.G., He, B., Chung, S.L., Menzies, M.A., Frey, F.A., 2004. The geologic, geochemical and geophysical consequences of plume involvement in the Emeishan flood basalt province. Geology 30, 917–920.
Xu, Y.G., He, B., Huang, X., Luo, Z., Chung, S.L., Xiao, L., Zhu, D., Shao, H., Fan, W.M., Xu, J.F., Wang, Y.J., 2007. Identification of mantle plumes in the Emeishan Large Igneous Province. Episodes 30 (1), 32–42.
Yogodzinski, G.M., Vervoort, J.D., Brown, S.T., Gerseny, M., 2010. Subduction controls of Hf and Nd isotopes in lavas of the Aleutian island arc. Earth Planet. Sci. Lett. 300, 226–238.
Yu, S.Y., Song, X.Y., Ripley, E., Li, C., Chen, L.M., 2015. Integrated O–Sr–Nd isotope constraints on the evolution of four important Fe–Ti oxide ore-bearing mafic–ultramafic intrusions in the Emeishan large igneous province, SW China. Chem. Geol. 401, 28–42.
Zhang, Z.C., Mahoney, J.J., Mao, J.W., Wang, F., 2006. Geochemistry of picritic and associated basalt flows of the western Emeishan flood basalt province, China. J. Petrol. 47, 1997–2019.
Zhang, M., Hu, P.Q., Niu, Y., Su, S.G., 2007. Chemical and stable isotopic constraints on the origin and nature of volatiles in sub-continental lithospheric mantle beneath eastern China. Lithos 96, 55–66.
Zhang, Z.C., Zhi, X.C., Chen, L., 2008. Re-Os isotopic compositions of picrites from the Emeishan flood basalt province, China. Earth Planet. Sci. Lett. 276, 30–39.
Zhang, M., Niu, Y., Hu, P., 2009. Volatiles in the mantle lithosphere: occurrence modes and chemical compositions. In: Anderson, J.E., Coates, R.W. (Eds.), The Lithosphere: Geochemistry, Geology and Geophysics. Nova Science Publishers, New York, pp. 171–212 (Chapter 5).
Zhang, M., Kamo, S.L., Li, C., Hu, P., Ripley, E.M., 2010. Precise U-Pb zircon-baddeleyite age of the Jinchuan sulfide ore-bearing ultramafic intrusion, western China. Mineral. Deposita 45 (1), 3–9.
Zhang, M., Li, C., Fu, P., Hu, P., Ripley, E.M., 2011. The Permian Huangshanxi Cu-Ni deposit in western China: intrusive-extrusive association, ore genesis, and exploration implications. Mineral. Deposita 46 (2), 153–170.
Zhang, M., Tang, Q., Hu, P., Ye, X., Cong, Y., 2013a. Noble gas isotopic constraints on the origin and evolution of the Jinchuan Ni-Cu-(PGE) sulfide ore-bearing ultramafic intrusion, Western China. Chem. Geol. 339, 301–312.
Zhang, Y., Ren, Z.-Y., Xu, Y.-G., 2013b. Sulfur in olivine-hosted melt inclusions from the Emeishan picrites. J. Geophys. Res. Solid Earth 118, 4063–4070.
Zhong, H., Zhu, W.G., Hu, R.Z., Xie, L.W., He, D.F., 2009. Zircon U-Pb age and Sr-Nd-Hf isotope geochemistry of the Panzhihua A-type syenitic intrusion in the Emeishan large igneous province, southwest China and implications for growth of juvenile crust. Lithos 110, 109–128.
Zhong, H., Campbell, I.H., Zhu, W.G., Allen, C.M., Hu, R.Z., Xie, L.W., He, D.F., 2011. Timing and source constraints on the relationship between mafic and felsic intrusions in the Emeishan large igneous province. Geochim. Cosmochim. Acta 75, 1374–1395.
Zhong, Y.T., He, B., Mundil, R., Xu, Y.G., 2014. CA-TIMS zircon U–Pb dating of felsic ignimbrite from the Binchuan section: implications for the termination age of Emeishan large igneous province. Lithos 204, 14–19.
Zhou, M.F., Robinson, P.T., Lesher, C.M., Keays, R.R., Zhang, C.J., Malpas, J., 2005. Geochemistry, petrogenesis and metallogenesis of the Panzhihua intrusion and associated Fe-Ti-V oxide deposits, Sichuan province, SW China. J. Petrol. 46, 2253–2280.
Zhou, M.F., Arndt, N.T., Malpas, J., Wang, C.Y., Kennedy, A., 2008. Two magma series and associated ore deposit types in the Permian Emeishan large igneous province, SW China. Lithos 103, 352–368.
Zindler, A., Hart, S.R., 1986. Chemical geodynamics. Annu. Rev. Earth Planet. Sci. 14, 493–571.